Cooperative MIMO Channel Modeling and Multi-Link Spatial Correlation Properties

Xiang Cheng[1], Cheng-Xiang Wang[2*], Haiming Wang[3], Xiqi Gao[3], Xiao-Hu You[3], Dongfeng Yuan[4], Bo Ai[5], Qiang Huo[1], Ling-Yang Song[1], and Bing-Li Jiao[1]

[1]Research Institute for Modern Communications
School of Electronics Engineering & Computer Science
Peking University, Beijing, 100871, China.
Email: {xiangcheng, qiang.huo, lingyang.song, jiaobl}@pku.edu.cn

[2]Joint Research Institute for Signal and Image Processing
School of Engineering & Physical Sciences
Heriot-Watt University, Edinburgh EH14 4AS, UK.
Email: cheng-xiang.wang@hw.ac.uk

[3] School of Information Science and Engineering
Southeast University, Najing, 210096, China.
Email: {hmwang, xqgao, xhyu}@seu.edu.cn

[4] School of Information Science and Engineering
Shandong University, Jinan, 250100, China.
Email: dfyuan@sdu.edu.cn

[5]State Key Laboratory of Rail Traffic Control and Safety
Beijing Jiaotong University, Beijing 100044, China.
Email: boai@bjtu.edu.cn

Submitted to IEEE Journal on Selected Areas in Communications, Special Issue on Cooperative Networking – Challenges and Applications.

*Correspondence author: Cheng-Xiang Wang, Tel: +44 131 4513329, Fax: +44 131 4514155.

The authors would like to acknowledge the support from the RCUK for the UK-China Science Bridges Project: R&D on (B)4G Wireless Mobile Communications. C.-X. Wang would also like to acknowledge the support by the Scottish Funding Council for the Joint Research Institute in Signal and Image Processing with the University of Edinburgh, as a part of the Edinburgh Research Partnership in Engineering and Mathematics (ERPem), and by the Opening Project of Key Laboratory of Cognitive Radio and Information Processing (Guilin University of Electronic Technology), Ministry of Education, under Grant 2009KF02. The work of H.-M. Wang was supported in part by the National Science and Technology Major Project of China under Grant 2009ZX03007-003-02.

Abstract

In this paper, a novel unified channel model framework is proposed for cooperative multiple-input multiple-output (MIMO) wireless channels. The proposed model framework is generic and adaptable to multiple cooperative MIMO scenarios by simply adjusting key model parameters. Based on the proposed model framework and using a typical cooperative MIMO communication environment as an example, we derive a novel geometry-based stochastic model (GBSM) applicable to multiple wireless propagation scenarios. The proposed GBSM is the first cooperative MIMO channel model that has the ability to investigate the impact of the local scattering density (LSD) on channel characteristics. From the derived GBSM, the corresponding multi-link spatial correlation functions are derived and numerically analyzed in detail. Numerical results indicate that some key channel model parameters have significant impacts on the resulting spatial correlation functions. The proposed cooperative MIMO channel model framework, GBSM, and the derived spatial correlation properties are helpful for better understanding cooperative MIMO channels and for setting up more purposeful measurement campaigns.

Index Terms

Cooperative MIMO channels, geometry-based stochastic model, spatial correlation, non-isotropic scattering, Ricean fading.

I. Introduction

Conventional multiple-input multiple-output (MIMO) technology, known as point-to-point MIMO, has been widely used in many standards [1], [2] due to its ability to significantly enhance the performance of wireless communication systems [3], [4]. Research on cooperative MIMO technologies has recently received much attention [5]– [11]. Cooperative MIMO, also known as virtual MIMO or distributed MIMO, groups multiple radio devices to form virtual antenna arrays so that they can cooperate with each other by exploiting the spatial domain of mobile fading channels. Due to the advantages of cooperative MIMO technology, such as improving coverage and cell edge throughput, it has been employed in some new wireless systems, e.g., cognitive radio networks [12], vehicular communication systems [13], and physical layer security systems [14]. Note that the cooperation of the grouped devices does not mean that the base station (BS) and mobile station (MS) have to be in reach of each other. Some devices can be treated as relays to help the communication between the BS and MS. As a new emerging technology, many research challenges in cooperative communications have to be addressed before the wide deployment. Detailed knowledge about the underlying propagation channels and the corresponding channel models are the fundamental to meet those challenges for the better design of cooperative MIMO systems [15].

Several papers have reported measurements of various statistical properties of cooperative MIMO channels for different scenarios. A few indoor cooperative channel measurements were reported in [16], [17], where the cooperative nodes are all static. Mobile multi-link measurements were presented in [18] for indoor cooperative MIMO channels. Outdoor cooperative MIMO channel measurements were addressed in [19], [20] and [21]– [23] for static nodes and mobile nodes, respectively. All these measurement campaigns concentrated on the investigation of the channel characteristics of individual links for different scenarios, such as path loss, shadow fading, and small scale fading. Unlike conventional point-to-point MIMO systems, cooperative MIMO systems consist of multiple radio links that may exhibit strong correlations, e.g., BS-BS, BS-relay station (RS), RS-RS, RS-MS, BS-MS, and MS-MS links. The correlation of multiple links exists due to the environment similarity arising from common shadowing objects and scatterers contributing to different links and can significantly affect the performance of cooperative MIMO systems. The investigation of the correlations between different links is rare in the current literature.

The multi-link correlation consists of large scale fading correlation and small scale fading correlation. Only a few papers have analyzed and modeled large scale fading correlations, including shadow fading correlation, delay spread correlation, and azimuth correlation. The 3rd Generation Partnership Project (3GPP) Spatial Channel Model (SCM) [24], the Wireless World Initiative New Radio Phase II (WINNER

II) channel model [25], and the IEEE 802.16j channel model [26] all investigated and modeled large scale fading correlations of different links for multiple scenarios. However, as mentioned in [27], these correlation models are not consistent and a unified correlation model for large scale fading is necessary. Recently, in [28] a unified framework that can investigate both static and dynamic shadow fading correlations was proposed for indoor and outdoor-to-indoor scenarios. There are even fewer papers available investigating small scale fading correlations. In [29], the authors proposed a multiuser MIMO channel model focusing on the investigation of the impact of surface roughness on spatial correlations. In [27], a preliminary investigation on spatial correlations for coordinated multi-point (CoMP) transmissions was reported. The investigation on spatial correlations of multi-link propagation channels in amplify-and-forward (AF) relay systems was reported in [30]. However, all the aforementioned investigations on multi-link spatial correlations are scenario-specific. For example, [29] only modeled the scenario where scatterers are located in streets, [27] only focused the CoMP scenario, and [30] only investigated the AF relay scenario. A unified channel model framework to investigate multi-link small scale fading correlations for different scenarios is therefore highly desirable.

To fill the aforementioned gap, this paper proposes a unified channel model framework for cooperative MIMO systems and investigates spatial correlations of different links in multiple scenarios. The main contributions and novelties of this paper are listed as follows.

1) We propose a wideband unified channel model framework that is suitable to mimic different links in cooperative MIMO systems, such as the BS-BS/RS/MS link, RS-RS/MS link, and MS-MS link. Due to different local scattering environments around BSs, RSs, and MSs, a high degree of link heterogeneity or variations is expected in cooperative MIMO systems. In this paper, we are interested in various cooperative MIMO environments which can be classified based on the physical scenarios and application scenarios. The physical scenarios include outdoor macro-cell, micro-cell, pico-cell, and indoor scenarios. Each physical scenario further includes 3 application scenarios, i.e., BS cooperation, MS cooperation, and relay cooperation. Therefore, 12 cooperative MIMO scenarios are considered in this paper and the proposed framework can be adapted to the 12 scenarios by simply adjusting key model parameters.
2) Taking a cooperative relay system, which includes three links (BS-RS, RS-MS, and BS-MS), as an example, we show how to apply the proposed channel model framework and derive a novel geometry-based stochastic model (GBSM) for multiple physical scenarios. The proposed GBSM is the first cooperative MIMO channel model that has the ability to mimic the impact of the local

scattering density (LSD) on channel characteristics.

3) From the proposed GBSMs, we further derive the multi-link spatial correlation functions that can significantly affect the performance of cooperative MIMO communication systems.
4) The impact of some important parameters, such as antenna element spacings and the LSDs, on multi-link spatial correlations in different scenarios is then investigated. Some interesting observations and conclusions are obtained, which can help better understand cooperative MIMO channels and thus better design cooperative MIMO systems.

The remainder of this paper is outlined as follows. Section II proposes the new unified channel model framework for cooperative wireless MIMO channels. The derivation of a new GBSM for wideband cooperative MIMO Ricean fading channels is given in Section III. In Section IV, based on the proposed GBSM, the multi-link spatial correlation functions are derived. Numerical results and analysis are presented in Section V. Finally, conclusions are drawn in Section VI.

II. A Unified Cooperative MIMO Channel Model Framework

Cooperative MIMO channel measurements [23], [28], [31] have clearly demonstrated that the degree of link heterogeneity in cooperative MIMO systems is highly related to local scattering environments around different devices. Therefore, the cooperative MIMO model framework needs to reflect the influence of different local scattering environments on the link heterogeneity for different scenarios while keeping the acceptable model complexity.

Let us now consider a general wideband cooperative MIMO system where all nodes are surrounded by local scatterers and a link between Node A and Node B is presented as shown in Fig. 1. It is assumed that each node can be in motion and is equipped with L antenna elements. The proposed unified channel model framework expresses the channel impulse response (CIR) between the pth antenna in Node A and the qth antenna in Node B as the superposition of line-of-sight (LoS) and scattered rays

$$h_{pq}\left(t,\tau\right)=h_{pq}^{LoS}\left(t,\tau\right)+\sum_{i=1}^{I}\sum_{g=1}^{f_I(i)}h_{pq}^{ig}\left(t,\tau\right) \tag{1}$$

where $I\geq 1$ is the number of related local scattering areas, $f_I(i)=\frac{I!}{(I-i)!\cdot i!}$ denotes the total number of i-bounced components, and $h_{pq}^{ig}\left(t,\tau\right)$ represents the gth scattered component consisting of i-bounced rays. For example, $h_{pq}^{21}\left(t,\tau\right)$ denotes the first double-bounced component. It is worth noting that the parameter $f_I(i)$ is obtained not purely based on the number of related local scattering areas, but also according to the following practical criterion: the i-bounced waves are always bounced by i scatterers located in different local scattering areas from far to near relative to the receiver. Based on this practical criterion,

some i-bounced components are not necessarily to be considered, which makes the proposed model more practical. For the cooperative communication environment shown in Fig. 1 with I=4, the proposed model framework consists of the LoS component, $f_4(1)$=4 single-bounced components, $f_4(2)$=6 double-bounced components, $f_4(3)$=4 triple-bounced components, and $f_4(4)$=1 quadruple-bounced component. While other multi-bounced components that violate the aforementioned practical criterion are not included in the proposed model framework, such as the $A_p - S_B - S_C - B_q$ double-bounced component.

In the proposed model framework (1), the LoS component of the CIR is deterministic and can be expressed as [32]

$$h_{pq}^{LoS}(t,\tau) = \sqrt{\frac{K_{pq}\Omega_{pq}}{K_{pq}+1}} e^{-j2\pi\lambda^{-1}\chi_{pq}} e^{j\left[2\pi f_{max}^{A} t\cos\left(\alpha_{pq}^{LoS}-\gamma_A\right)+2\pi f_{max}^{B} t\cos\left(\phi_{pq}^{LoS}-\gamma_B\right)\right]}\delta(\tau-\tau_{LoS}) \tag{2}$$

where χ_{pq} is the travel path of the LoS waves through the link between A_p and B_q (A_p–B_q link), τ_{LoS} denotes the LoS time delay, and λ is the wave length with $\lambda = c/f$ where c is the speed of light and f is the carrier frequency. The symbols K_{pq} and Ω_{pq} designate the Ricean factor and the total power of the A_p–B_q link, respectively. Parameters f_{max}^{A} and f_{max}^{B} are the maximum Doppler frequency with respect to Node A and Node B, respectively, γ_A and γ_B are the angles of motion with respect to Node A and Node B, respectively, and α_{pq}^{LoS} and ϕ_{pq}^{LoS} denote the angles of arrival/departure of the LoS path with respect to Node A and Node B, respectively. The scattered component of the CIR in (1) can be shown as [32]

$$\begin{aligned} h_{pq}^{ig}(t,\tau) &= \sqrt{\frac{\eta_{pq}^{ig}\Omega_{pq}}{K_{pq}+1}} \lim_{\{N_k^g\}_{k=1}^{i}\to\infty} \sum_{\{n_k^g\}_{k=1}^{i}=1}^{\{N_k^g\}_{k=1}^{i}} \frac{1}{\sqrt{\prod_{k=1}^{i} N_k^g}} e^{j\left(\psi_{\{n_k^g\}_{k=1}^{i}} - 2\pi\lambda^{-1}\chi_{pq,\{n_k^g\}_{k=1}^{i}}\right)} \\ &\quad \times e^{j\left[2\pi f_{max}^{A} t\cos\left(\alpha_{pq,\{n_k^g\}_{k=1}^{i}}-\gamma_A\right)+2\pi f_{max}^{B} t\cos\left(\phi_{pq,\{n_k^g\}_{k=1}^{i}}-\gamma_B\right)\right]}\delta(\tau-\tau_{\{n_k^g\}_{k=1}^{i}}) \end{aligned} \tag{3}$$

where N_k^g is the number of effective scatterers in the kth local scattering area with respect to the gth i-bounced component, $\{\chi_{pq,n_k^g}\}_{k=1}^{i}$ is the travel path of the gth i-bounced waves through the A_p–B_q link, $\{\tau_{n_k^g}\}_{k=1}^{i}$ denotes the time delay of the multipath components. The phases $\{\psi_{n_k}\}_{k=1}^{i}$ are independent and identically distributed (i.i.d.) random variables with uniform distributions over $[-\pi,\pi)$ and determined by scatterers $\{S_{n_K}\}_{k=1}^{i}$, $\{X_{n_k}\}_{k=1}^{i}$ represents $X_{n_1}, X_{n_2}, X_{n_3}, ..., X_{n_i}$, and $\{\alpha_{pq,n_k^g}\}_{k=1}^{i}$ and $\{\phi_{pq,n_k^g}\}_{k=1}^{i}$ denote angles of arrival/departure of a i-bounced path with respect to Node A and Node B, respectively. Here, η_{pq}^{ig} is a energy-related parameter specifying how much the gth i-bounced rays contribute to the total scattered power $\Omega_{pq}/(K_{pq}+1)$. Note that energy-related parameters satisfy $\sum_{i=1}^{I}\sum_{g=1}^{f_I(i)}\eta_{pq}^{ig}=1$.

It is clear that the proposed unified channel model framework in (1) can naturally include the impact of local scattering area on channel characteristics with the help of properly choosing $f_I(i)$ i-bounced

components. Note that parameter $f_I(i)$ is related to the number of related local scattering areas I, which is determined by physical environments, outdoor macro-cell, micro-cell, pico-cell, and indoor. This means by properly adjusting the parameter I, the proposed model framework is suitable for different basic cooperative environments. Furthermore, the proposed model framework can model multiple links with different degrees of link heterogeneity due to different application scenes (e.g., BS cooperation, MS cooperation, and relay cooperation) for a typical cooperative environment by simply adjusting the Ricean factor K_{pq} and energy-related parameters η_{pq}^{ig}. How to properly set these key model parameters, i.e., I, K_{pq}, η_{pq}^{ig}, will be explained in the next section where the proposed unified cooperative channel model framework is implemented for a typical cooperative MIMO application scenario.

III. A New MIMO GBSM for Cooperative Relay Systems

Without loss of generality, this section considers a wideband cooperative relay communication environment that includes three different links: BS-RS, RS-MS, and BS-MS, to implement the proposed cooperative MIMO channel model framework. Note that the designed cooperative MIMO GBSM can be easily extended to other cooperative MIMO scenarios with multiple relays. The RS can be another BS for BS cooperation or another MS for MS cooperation. In order to propose a generic cooperative MIMO GBSM that is suitable for the aforementioned 12 cooperative scenarios, we assume that the BS, RS, and MS are all surrounded by local scatterers. Fig. 2 shows the geometry of the proposed cooperative MIMO GBSM, combining the LoS components and scattered components. To keep the readability of Fig. 2, the LoS components are not shown. It is assumed that the BS, RS, and MS are all equipped with $A_B = A_R = A_M = 2$ uniform linear antenna arrays. The local scattering environment is characterized by the effective scatterers located on circular rings. Suppose there are N_1 effective scatterers around the MS lying on a circular ring of radius $R_{1n_1} \leq \xi_{n_1}^M \leq R_{1n_2}$ and the n_1th ($n_1 = 1, ..., N_1$) effective scatterer is denoted by S_{n_1}. Similarly, assume there are N_2 effective scatterers around the RS lying on a circular ring of radius $R_{2n_1} \leq \xi_{n_2}^R \leq R_{2n_2}$ and the n_2th ($n_2 = 1, ..., N_2$) effective scatterer is denoted by S_{n_2}. For the local scattering area around BS, N_3 effective scatterers lie on a circular ring of radius $R_{3n_1} \leq \xi_{n_3}^B \leq R_{3n_2}$ and the n_3th ($n_3 = 1, ..., N_3$) effective scatterer is denoted by S_{n_3}. The parameters in Fig. 2 are defined in Table I.

As this paper only focuses on the investigation of multi-link spatial correlations (not time or frequency correlations), we will neglect t and τ in (1) for the proposed channel model framework to simplify notations. In the following, we will show the channel gains of the three different links for the proposed cooperative MIMO GBSM.

A. BS-RS link

The channel gain of the BS-RS link between Antenna p_3 at the BS and Antenna p_2 at the RS can be expressed as

$$h_{p_3p_2} = h_{p_3p_2}^{LoS} + \sum_{i=1}^{3}\sum_{g=1}^{f_3(i)} h_{p_3p_2}^{ig} \tag{4}$$

where $h_{p_3p_2}^{LoS}$ denotes the LoS component and $h_{p_3p_2}^{ig}$ represents the gth i-bounced component with the following expressions

$$h_{p_3p_2}^{LoS} = \sqrt{\frac{K_{p_3p_2}\Omega_{p_3p_2}}{K_{p_3p_2}+1}} e^{-j2\pi\lambda^{-1}\chi_{p_3p_2}} \tag{5}$$

$$h_{p_3p_2}^{1g} = \sqrt{\frac{\eta_{p_3p_2}^{1g}\Omega_{p_3p_2}}{K_{p_3p_2}+1}} \lim_{N_g\to\infty}\sum_{n_g=1}^{N_g}\frac{1}{\sqrt{N_g}} e^{j\left(\psi_{n_g}-2\pi\lambda^{-1}\chi_{p_3p_2,n_g}\right)} \tag{6}$$

$$h_{p_3p_2}^{2g} = \sqrt{\frac{\eta_{p_3p_2}^{2g}\Omega_{p_3p_2}}{K_{p_3p_2}+1}} \lim_{N_{g_1},N_{g_2}\to\infty}\sum_{n_{g_1},n_{g_2}=1}^{N_{g_1},N_{g_2}}\frac{1}{\sqrt{N_{g_1}N_{g_2}}} e^{j\left(\psi_{n_{g_1},n_{g_2}}-2\pi\lambda^{-1}\chi_{p_3p_2,n_{g_1},n_{g_2}}\right)} \tag{7}$$

$$h_{p_3p_2}^{31} = \sqrt{\frac{\eta_{p_3p_2}^{31}\Omega_{p_3p_2}}{K_{p_3p_2}+1}} \lim_{N_1,N_2,N_3\to\infty}\sum_{n_1,n_2,n_3=1}^{N_1,N_2,N_3}\frac{1}{\sqrt{N_1N_2N_3}} e^{j\left(\psi_{n_1,n_2,n_3}-2\pi\lambda^{-1}\chi_{p_3p_2,n_1,n_2,n_3}\right)} \tag{8}$$

where $g=1,2,3$, $\{g_1,g_2\}=\{3,2\}$ for $g=1$, $\{g_1,g_2\}=\{3,1\}$ for $g=2$, and $\{g_1,g_2\}=\{1,2\}$ for $g=3$. In (5)–(8), $\chi_{p_3p_2}=\varepsilon_{p_3p_2}$, $\chi_{p_3p_2,n_g}=\varepsilon_{p_3n_g}+\varepsilon_{n_gp_2}$, $\chi_{p_3p_2,n_{g_1},n_{g_2}}=\varepsilon_{p_3n_{g_1}}+\varepsilon_{n_{g_1}n_{g_2}}+\varepsilon_{n_{g_2}p_2}$, and $\chi_{p_3p_2,n_1,n_2,n_3}=\varepsilon_{p_3n_3}+\varepsilon_{n_3n_1}+\varepsilon_{n_1n_2}+\varepsilon_{n_2p_2}$ are the travel times of the waves through the link $B_{p_3}-R_{p_2}$, $B_{p_3}-S_{n_g}-R_{p_2}$, $B_{p_3}-S_{n_{g_1}}-S_{n_{g_2}}-R_{p_2}$, and $B_{p_3}-S_{n_3}-S_{n_1}-S_{n_2}-R_{p_2}$, respectively. The symbols $K_{p_3p_2}$ and $\Omega_{p_3p_2}$ designate the Ricean factor and the total power of the BS-RS link, respectively. Parameters $\eta_{p_3p_2}^{1g}$, $\eta_{p_3p_2}^{2g}$, and $\eta_{p_3p_2}^{31}$ specify how much the single-, double-, and triple-bounced rays contribute to the total scattered power $\Omega_{p_3p_2}/(K_{p_3p_2}+1)$ with $\sum_{g=1}^{3}(\eta_{p_3p_2}^{1g}+\eta_{p_3p_2}^{2g})+\eta_{p_3p_2}^{31}=1$. The phases ψ_{n_g}, $\psi_{n_{g_1},n_{g_2}}$, and ψ_{n_1,n_2,n_3} are i.i.d. random variables with uniform distributions over $[-\pi,\pi)$.

From Fig. 2 and based on the normally used assumption $\min\{D_1,D_2,D_3\}\gg\max\{\delta_1,\delta_2,\delta_3\}$ [32] and the application of the law of cosines in appropriate triangles, the distances $\varepsilon_{p_3p_2}$, $\varepsilon_{p_3n_g}$, $\varepsilon_{n_gp_2}$, $\varepsilon_{n_1n_2}$, $\varepsilon_{n_3n_2}$, and $\varepsilon_{n_3n_1}$ in (5)–(8) can be expressed as

$$\varepsilon_{p_3p_2} \approx D_3 - \frac{\delta_3}{2}\cos(\beta_3-\theta') + \frac{\delta_2}{2}\cos(\beta_2-\theta') \tag{9}$$

$$\varepsilon_{p_3n_g} \approx \xi_{n_g}^{B} - \frac{\delta_3}{2}\cos(\beta_3-\alpha_{1n_g}) \tag{10}$$

$$\varepsilon_{n_gp_2} \approx \xi_{n_g}^{R} - \frac{\delta_2}{2}\cos(\beta_2-\alpha_{2n_g}) \tag{11}$$

$$\varepsilon_{n_1n_2} = \left[(\xi_{n_1}^{R})^2+(\xi_{n_2}^{R})^2-2\xi_{n_1}^{R}\xi_{n_2}^{R}\cos(\alpha_{2n_1}-\alpha_{2n_2})\right]^{1/2} \tag{12}$$

$$\varepsilon_{n_3 n_\varrho} = [(\xi^B_{n_3})^2 + (\xi^B_{n_\varrho})^2 - 2\xi^B_{n_3}\xi^B_{n_\varrho}\cos(\alpha_{3n_3} - \alpha_{1n_\varrho})]^{1/2} \tag{13}$$

where $\xi^B_{n_1} = \sqrt{D_1^2 + (\xi^M_{n_1})^2 + 2D_1\xi^M_{n_1}\cos\alpha_{1n_1}}$, $\xi^R_{n_1} = \sqrt{D_2^2 + (\xi^M_{n_1})^2 + 2D_2\xi^M_{n_1}\cos(\alpha_{1n_1} + \theta)}$, $\xi^B_{n_2} = \sqrt{D_3^2 + (\xi^R_{n_2})^2 + 2D_3\xi^R_{n_2}\cos(\alpha_{2n_2} - \theta')}$, $\xi^R_{n_3} = \sqrt{D_3^2 + (\xi^B_{n_3})^2 - 2D_3\xi^B_{n_3}\cos(\alpha_{3n_3} - \theta')}$, $\xi^R_{n_2} \in [R_{1n_2}, R_{2n_2}]$, $\xi^B_{n_3} \in [R_{1n_3}, R_{2n_3}]$, $\varrho = 1, 2$, and g=1, 2, 3. Note that the AoD α_{3n_1}, α_{3n_2}, α_{3n_3} and AoA α_{2n_1}, α_{2n_2}, α_{2n_3} are independent for double- and triple-bounced rays, while they are interdependent for single-bounced rays. It is worth highlighting that scatterers S_{n_g} around MS, RS, and BS are relevant to the angles α_{1n_1}, α_{2n_2}, and α_{3n_3}, respectively. Therefore, all other AoDs and AoAs have to be related to the aforementioned three key angles. By following the general method given in [32], the relationship of the key angles with other AoAs and AoDs of BS-RS link can be obtained as: $\sin\alpha_{3n_1} = \frac{\xi^M_{n_1}}{\xi^B_{n_1}}\sin\alpha_{1n_1}$, $\sin(\alpha_{2n_1} + \theta) = \frac{\xi^M_{n_1}}{\xi^R_{n_1}}\sin(\theta + \alpha_{1n_1})$, $\sin(\alpha_{3n_2} - \theta') = \frac{\xi^R_{n_2}}{\xi^B_{n_2}}\sin(\alpha_{2n_2} - \theta')$, and $\sin(\alpha_{2n_3} - \theta') = \frac{\xi^B_{n_3}}{\xi^R_{n_3}}\sin(\alpha_{3n_3} - \theta')$.

Note that the above derived distances and angles have general expressions and thus are suitable for various basic scenarios. For outdoor macro-cell and micro-cell scenarios, the assumption $\min\{D_1, D_2, D_3\} \gg \max\{\xi^M_{n_1}, \xi^R_{n_2}, \xi^B_{n_3}\}$, which is invalid for outdoor pico-cell scenario and indoor scenario, is fulfilled. Therefore, for outdoor macro-cell and micro-cell scenarios, we have the following reduced expressions: $\varepsilon_{n_1 n_2} \approx D_2$, $\varepsilon_{n_3 n_2} \approx D_3$, $\varepsilon_{n_3 n_1} \approx D_1$, $\xi^B_{n_1} \approx D_1 + \xi^M_{n_1}\cos\alpha_{1n_1}$, $\xi^R_{n_1} \approx D_2 + \xi^M_{n_1}\cos(\alpha_{1n_1} + \theta)$, $\xi^B_{n_2} \approx D_3 + \xi^R_{n_2}\cos(\alpha_{2n_2} - \theta')$, $\xi^R_{n_3} \approx D_3 - \xi^B_{n_3}\cos(\alpha_{3n_3} - \theta')$, $\alpha_{3n_1} \approx \frac{\xi^M_{n_1}}{D_1}\sin\alpha_{1n_1}$, $\alpha_{2n_1} \approx 2\pi - \theta + \frac{\xi^M_{n_1}}{D_2}\sin(\theta + \alpha_{1n_1})$, $\alpha_{3n_2} \approx \theta' - \frac{\xi^R_{n_2}}{D_3}\sin(\alpha_{2n_2} - \theta')$, and $\alpha_{2n_3} \approx \pi + \theta' - \frac{\xi^B_{n_3}}{D_3}\sin(\alpha_{3n_3} - \theta')$.

B. BS-MS link

The channel gain of BS-MS link between antenna p_3 at BS and antenna p_1 at MS can be expressed as

$$h_{p_3 p_1} = h^{LoS}_{p_3 p_1} + \sum_{i=1}^{3}\sum_{g=1}^{f_3(i)} h^{ig}_{p_3 p_1} \tag{14}$$

where $h^{LoS}_{p_3 p_1}$ denotes the LoS component and $h^{ig}_{p_3 p_1}$ represents the gth i-bounced component with the following expressions

$$h^{LoS}_{p_3 p_1} = \sqrt{\frac{K_{p_3 p_1}\Omega_{p_3 p_1}}{K_{p_3 p_1} + 1}} e^{-j2\pi\lambda^{-1}\chi_{p_3 p_1}} \tag{15}$$

$$h^{1g}_{p_3 p_1} = \sqrt{\frac{\eta^{1g}_{p_3 p_1}\Omega_{p_3 p_1}}{K_{p_3 p_1} + 1}} \lim_{N_g \to \infty} \sum_{n_g=1}^{N_g} \frac{1}{\sqrt{N_g}} e^{j\left(\psi_{n_g} - 2\pi\lambda^{-1}\chi_{p_3 p_1, n_g}\right)} \tag{16}$$

$$h^{2g}_{p_3 p_1} = \sqrt{\frac{\eta^{2g}_{p_3 p_1}\Omega_{p_3 p_1}}{K_{p_3 p_1} + 1}} \lim_{N_{g_1}, N_{g_2} \to \infty} \sum_{n_{g_1}, n_{g_2}=1}^{N_{g_1}, N_{g_2}} \frac{1}{\sqrt{N_{g_1} N_{g_2}}} e^{j\left(\psi_{n_{g_1}, n_{g_2}} - 2\pi\lambda^{-1}\chi_{p_3 p_1, n_{g_1}, n_{g_2}}\right)} \tag{17}$$

$$h^{31}_{p_3 p_1} = \sqrt{\frac{\eta^{31}_{p_3 p_1}\Omega_{p_3 p_1}}{K_{p_3 p_1} + 1}} \lim_{N_1, N_2, N_3 \to \infty} \sum_{n_1, n_2, n_3=1}^{N_1, N_2, N_3} \frac{1}{\sqrt{N_1 N_2 N_3}} e^{j\left(\psi_{n_1, n_2, n_3} - 2\pi\lambda^{-1}\chi_{p_3 p_1, n_1, n_2, n_3}\right)} \tag{18}$$

where parameters g, g_1, and g_2 are the same as the ones in (5)–(8). In (15)–(18), $\chi_{p_3p_1}=\varepsilon_{p_3p_1}$, $\chi_{p_3p_1,n_g}=\varepsilon_{p_3n_g}+\varepsilon_{n_gp_1}$, $\chi_{p_3p_1,n_{g_1},n_{g_2}}=\varepsilon_{p_3n_{g_1}}+\varepsilon_{n_{g_1}n_{g_2}}+\varepsilon_{n_{g_2}p_1}$, and $\chi_{p_3p_1,n_1,n_2,n_3}=\varepsilon_{p_3n_3}+\varepsilon_{n_3n_2}+\varepsilon_{n_2n_1}+\varepsilon_{n_1p_1}$ are the travel times of the waves through the link $B_{p_3}-M_{p_1}$, $B_{p_3}-S_{n_g}-M_{p_1}$, $B_{p_3}-S_{n_{g_1}}-S_{n_{g_2}}-M_{p_1}$, and $B_{p_3}-S_{n_3}-S_{n_2}-S_{n_1}-M_{p_1}$, respectively. The symbols $K_{p_3p_1}$ and $\Omega_{p_3p_1}$ designate the Ricean factor and the total power of the BS-MS link, respectively. Parameters $\eta^{1g}_{p_3p_1}$, $\eta^{2g}_{p_3p_1}$, and $\eta^{31}_{p_3p_1}$ specify how much the single-, double-, and triple-bounced rays contribute to the total scattered power $\Omega_{p_3p_1}/(K_{p_3p_1}+1)$ with $\sum_{g=1}^{3}(\eta^{1g}_{p_3p_1}+\eta^{2g}_{p_3p_1})+\eta^{31}_{p_3p_1}=1$. The phases ψ_{n_1,n_3} is i.i.d. random variable with uniform distributions over $[-\pi,\pi)$.

Similar to the BS-RS link, by applying of the law of cosines in appropriate triangles, we have the following expressions of the desired distances with the help of the normally used assumption $\min\{D_1,D_2,D_3\}\gg\max\{\delta_1\delta_2,\delta_3\}$

$$\varepsilon_{p_3p_1} \approx D_1-\frac{\delta_3}{2}\cos\beta_3+\frac{\delta_1}{2}\cos(\beta_1) \tag{19}$$

$$\varepsilon_{n_gp_1} \approx \xi^M_{n_g}-\frac{\delta_1}{2}\cos(\beta_1-\phi_{n_g}) \tag{20}$$

where $g=1,2,3$, $\xi^M_{n_1}\in[R_{1n_1},R_{2n_1}]$, $\xi^M_{n_2}=\sqrt{D_2^2+(\xi^R_{n_2})^2-2D_2\xi^R_{n_2}\cos\varphi_{n_2}}$ with $\varphi_{n_2}=2\pi-\theta'-\alpha_{2n_2}$, and $\xi^M_{n_3}=\sqrt{D_1^2+(\xi^B_{n_3})^2-2D_1\xi^B_{n_3}\cos\alpha_{3n_3}}$. The expressions of other interested distances $\varepsilon_{p_3n_1}$, $\varepsilon_{p_3n_2}$, $\varepsilon_{p_3n_3}$, $\varepsilon_{n_3n_1}$, $\varepsilon_{n_3n_2}$, and $\varepsilon_{n_2n_1}=\varepsilon_{n_1n_2}$ have been given previously in the BS-RS link. Similar to the BS-RS link, angles α_{1n_2} and α_{1n_3} need to be related to any one of three key angles as $\sin(\alpha_{1n_2}+\theta)=\frac{\xi^R_{n_2}}{\xi^M_{n_2}}\sin(\alpha_{2n_2}+\theta)$ and $\sin\alpha_{1n_3}=\frac{\xi^B_{n_3}}{\xi^M_{n_3}}\sin\alpha_{3n_3}$.

Similar to the BS-RS link, the above derived expressions of the distances and angles are applicable to various basic scenarios. For outdoor macro-cell and micro-cell scenarios, by using the assumption $\min\{D_1,D_2,D_3\}\gg\max\{\xi^M_{n_1},\xi^R_{n_2},\xi^B_{n_3}\}$, the following reduced expressions can be obtained as: $\xi^M_{n_2}\approx D_2-\xi^R_{n_2}\cos\varphi_{n_2}$ with $\varphi_{n_2}=2\pi-(\alpha_{2n_2}+\theta)$, $\xi^M_{n_3}\approx D_1-\xi^B_{n_3}\cos\alpha_{3n_3}$, $\alpha_{1n_2}\approx\pi-\theta-\frac{\xi^R_{n_2}}{D_2}\sin(\theta+\alpha_{2n_2})$, and $\alpha_{1n_3}\approx\pi-\frac{\xi^B_{n_3}}{D_1}\sin\alpha_{3n_3}$.

C. RS-MS link

The channel gain of RS-MS link between antenna p_2 at BS and antenna p_1 at MS can be expressed as

$$h_{p_2p_1}=h^{LoS}_{p_2p_1}+\sum_{i=1}^{3}\sum_{g=1}^{f_3(i)}h^{ig}_{p_2p_1} \tag{21}$$

where $h^{LoS}_{p_2p_1}$ denotes the LoS component and $h^{ig}_{p_2p_1}$ represents the gth i-bounced component with the following expressions

$$h_{p_2p_1}^{LoS} = \sqrt{\frac{K_{p_2p_1}\Omega_{p_2p_1}}{K_{p_2p_1}+1}}e^{-j2\pi\lambda^{-1}\chi_{p_2p_1}} \tag{22}$$

$$h_{p_2p_1}^{1g} = \sqrt{\frac{\eta_{p_2p_1}^{1g}\Omega_{p_2p_1}}{K_{p_2p_1}+1}}\lim_{N_g\to\infty}\sum_{n_g=1}^{N_g}\frac{1}{\sqrt{N_g}}e^{j\left(\psi_{n_g}-2\pi\lambda^{-1}\chi_{p_2p_1,n_g}\right)} \tag{23}$$

$$h_{p_2p_1}^{2g} = \sqrt{\frac{\eta_{p_2p_1}^{2g}\Omega_{p_2p_1}}{K_{p_2p_1}+1}}\lim_{N_{g_1},N_{g_2}\to\infty}\sum_{n_{g_1},n_{g_2}=1}^{N_{g_1},N_{g_2}}\frac{1}{\sqrt{N_{g_1}N_{g_2}}}e^{j\left(\psi_{n_{g_1},n_{g_2}}-2\pi\lambda^{-1}\chi_{p_2p_1,n_{g_1},n_{g_2}}\right)} \tag{24}$$

$$h_{p_2p_1}^{31} = \sqrt{\frac{\eta_{p_2p_1}^{31}\Omega_{p_2p_1}}{K_{p_2p_1}+1}}\lim_{N_1,N_2,N_3\to\infty}\sum_{n_1,n_2,n_3=1}^{N_1,N_2,N_3}\frac{1}{\sqrt{N_1N_2N_3}}e^{j\left(\psi_{n_1,n_2,n_3}-2\pi\lambda^{-1}\chi_{p_2p_1,n_1,n_2,n_3}\right)} \tag{25}$$

where parameters g, g_1, and g_2 are the same as the ones in (5)–(8). In (22)–(25), $\chi_{p_2p_1}=\varepsilon_{p_2p_1}$, $\chi_{p_2p_1,n_g}=\varepsilon_{p_2n_g}+\varepsilon_{n_gp_1}$, $\chi_{p_2p_1,n_{g_1},n_{g_2}}=\varepsilon_{p_2n_{g_1}}+\varepsilon_{n_{g_1}n_{g_2}}+\varepsilon_{n_{g_2}p_1}$, and $\chi_{p_2p_1,n_1,n_2,n_3}=\varepsilon_{p_2n_2}+\varepsilon_{n_2n_3}+\varepsilon_{n_3n_1}+\varepsilon_{n_1p_1}$ are the travel times of the waves through the link R_{p_2}–M_{p_1}, R_{p_2}–S_{n_g}–M_{p_1}, R_{p_2}–$S_{n_{g_1}}$–$S_{n_{g_2}}$–M_{p_1}, and R_{p_2}–$S^{(n_2)}$–$S^{(n_3)}$–$S^{(n_1)}$–M_{p_1}, respectively. The symbols $K_{p_2p_1}$ and $\Omega_{p_2p_1}$ designate the Ricean factor and the total power of the RS-MS link, respectively. Parameters $\eta_{p_2p_1}^{1g}$, $\eta_{p_2p_1}^{2g}$, and $\eta_{p_2p_1}^{31}$ specify how much the single-, double-, and triple-bounced rays contribute to the total scattered power $\Omega_{p_2p_1}/(K_{p_2p_1}+1)$ with $\sum_{g=1}^{3}(\eta_{p_2p_1}^{1g}+\eta_{p_2p_1}^{2g})+\eta_{p_2p_1}^{31}=1$.

From Fig. 2, it is clear that all the expressions of the desired distances have been given previously in BS-RS and BS-MS links except the distance $\varepsilon_{p_2p_1}$ with the following expression $\varepsilon_{p_2p_1}\approx D_2-\frac{\delta_2}{2}\cos(\beta_2+\theta)-\frac{\delta_1}{2}\cos(\beta_1-\theta)$ where the assumption $D_2\gg\max\{\delta_2,\delta_1\}$ is utilized.

In the literature, different scatterer distributions have been proposed to characterize the key angles α_{1n_1}, α_{2n_2}, and α_{3n_3}, such as the uniform, Gaussian, wrapped Gaussian, and cardioid PDFs [33]. In this paper, the von Mises PDF [34] is used, which is more generic and can approximate all the aforementioned PDFs [32]. The von Mises PDF is defined as $f(\phi)\stackrel{\Delta}{=}\exp[k\cos(\phi-\mu)]/[2\pi I_0(k)]$, where $\phi\in[-\pi,\pi)$, $I_0(\cdot)$ is the zeroth-order modified Bessel function of the first kind, $\mu\in[-\pi,\pi)$ accounts for the mean value of the angle ϕ, and k ($k\geq 0$) is a real-valued parameter that controls the angle spread of the angle ϕ. In this paper, for the key angles, i.e., the α_{1n_1}, α_{2n_2}, and α_{3n_3}, we use appropriate parameters (μ and k) of the von Mises PDF as μ_1 and k_1, μ_2 and k_2, and μ_3 and k_3, respectively.

D. Adjustment of Key Model Parameters

The proposed cooperative MIMO GBSM is adaptable to the above mentioned 12 cooperative scenarios for this interested typical cooperative MIMO environment by adjusting key model parameters. From previous section, we know that these important model parameters are the number of local scattering environment I, Ricean factors $K_{p_3p_2}$, $K_{p_3p_1}$, $K_{p_2p_1}$, and energy-related parameters $\eta_{p_3p_2}^{ig}$, $\eta_{p_3p_1}^{ig}$, and $\eta_{p_2p_1}^{ig}$.

The paramter setting of I is basically based on basic scenario. For outdoor micro-cell, pico-cell, and indoor scenarios, we assume that the BS, RS, and MS are all surrounded by local scattering area as shown in Fig. 2 and thus $I = 3$ in this case. For outdoor Marco-cell scenario, the BS is free of scatterers and thus $I = 2$. In this case, the channel model can also be obtained from the proposed model in (4), (14), and (21) by setting the energy-related parameters related to the local scatterers around BS equal to zero, e.g., for BS-RS link, the channel model can be obtained from (4) by setting $\eta^{13}_{p_3p_2} = \eta^{21}_{p_3p_2} = \eta^{22}_{p_3p_2} = \eta^{31}_{p_3p_2} = 0$. For outdoor macro-cell BS cooperation scenario, RS actually represents the other BS, symbolled as BS2, and thus is free of scatterers as well. In this case, we have the currently most mature cooperative MIMO scheme: CoMP and the number of local scattering area $I = 1$. Similarly, the channel model with $I = 1$ can also be obtained from the proposed model in (4), (14), and (21) by setting the energy-related parameters related to the local scatterers around BS and RS(BS2) equal to zero. It is clear that the proposed GBSM can be adaptable to different basic scenarios by setting relevant energy-related parameters equal to zero. Therefore, the key model parameters of the proposed GBSM actually are reduced as the Ricean factors and energy-related parameters. The basic criterion of setting these key model parameters is summarized as following: the longer distance of the link and/or the higher the LSD, the smaller the Ricean factors and the larger the energy-related parameters of multi-bounced components, i.e., the multi-bounced components bear more energy than single-bounced components. Since the local scattering area is highly related to the degree of link heterogeneity in cooperative MIMO systems as presented in [23], [28], [31], the LSD significantly affects the channel characteristics and should be investigated. In general, the higher the LSD, the lower the possibility that the devices (BS/MS/RS) share the same scatterers. In this case, the cooperative MIMO environments present lower environment similarity. Therefore, the higher the LSD, the lower the environment similarity.

For macro-cell scenarios, the Ricean factor $K_{p_3p_1}$ is very small or even close to zero due to the large distance D_1. Under the condition of BS cooperation scenes, Ricean factor $K_{p_2p_1}$ is similar to $K_{p_3p_1}$ due to the similar distances of D_1 and D_2. While the BS-RS link is disappeared and replaced by wired link. In this case, we only have single bounced components, i.e., $\eta^{11}_{p_3p_1}$ and $\eta^{11}_{p_2p_1}$. For MS/RS cooperation scenes, RS/MS actually represents the other MS/RS and is symbolled as MS2/RS2. In this case, Ricean factor $K_{p_3p_2}$ is similar to $K_{p_3p_1}$ due to the similar distances of D_1 and D_3. Since the large value of distances D_1 and D_3, for the BS-MS/BR2 link and BS-MS2/RS link, the impact of LSD on channel characteristics is small and in general the double-bounced rays bear more energy than single-bounced rays, i.e., $\{\eta^{21}_{p_3p_1}, \eta^{21}_{p_3p_2}\} > \{\eta^{11}_{p_3p_1}, \eta^{12}_{p_3p_1}, \eta^{11}_{p_3p_2}, \eta^{12}_{p_3p_2}\}$. While for the MS/RS2-MS2/RS link, due to the small distance of D_2 the impact of LSD is significant. For a low LSD, the scatterers are sparse and thus

more likely single-bounced rays rather than double-bounced rays, i.e., $\{\eta^{11}_{p_2p_1}, \eta^{12}_{p_2p_1}\} > \eta^{21}_{p_2p_1}$, and Ricean factor $K_{p_2p_1}$ is large. For a high LSD, the double-bounced components bear more energy than single-bounced components, i.e., $\eta^{21}_{p_2p_1} > \{\eta^{11}_{p_2p_1}, \eta^{12}_{p_2p_1}\}$ and Ricean factor $K_{p_2p_1}$ is smaller than that in the low LSD. Similar to macro-cell scenarios, the key model parameters setting for other 9 cooperative scenarios with the consideration of different LSDs can be easily obtained by following the aforementioned basic criterion and thus omits here for brevity. The main features of the proposed cooperative MIMO GBSM have been summarized in Table II.

IV. Multi-link Spatial Correlation Functions

In this section, based on the proposed cooperative MIMO GBSM in Section III, we will derive the multi-link spatial correlation functions for non-isotropic scattering cooperative MIMO environments. The spatial correlation properties between any two of the aforementioned three links, i.e., BS-RS link, BS-MS link, and RS-MS link, will be investigated. The normalized spatial correlation function between any two links characterized by channel gains h_{pq} and $h_{p'q'}$, respectively, is defined as

$$\rho_{pq,p'q'} = \frac{\mathbf{E}\left[h_{pq}h^*_{p'q'}\right]}{\sqrt{\Omega_{pq}\Omega_{p'q'}}} \tag{26}$$

where $(\cdot)^*$ denotes the complex conjugate operation, $\mathbf{E}[\cdot]$ is the statistical expectation operator, $p, p' \in \{1, 2, ..., M_T\}$, and $q, q' \in \{1, 2, ..., M_R\}$. Substituting (4) and (14) into (26), we have the correlation function between BS-RS link and BS-MS link as

$$\rho_{p_3p_2,p'_3p_1} = \rho^{LoS}_{p_3p_2,p'_3p_1} + \sum_{g=1}^{3}(\rho^{1g}_{p_3p_2,p'_3p_1} + \rho^{2g}_{p_3p_2,p'_3p_1}) + \rho^{31}_{p_3p_2,p'_3p_1} \tag{27}$$

with

$$\rho^{LoS}_{p_3p_2,p'_3p_1} = \sqrt{\frac{K_{p_3p_2}K_{p'_3p_1}}{(K_{p_3p_2}+1)\left(K_{p'_3p_1}+1\right)}}e^{j2\pi\lambda^{-1}\left(\chi_{p'_3p_1}-\chi_{p_3p_2}\right)} \tag{28}$$

$$\rho^{1g}_{p_3p_2,p'_3p_1} = \sqrt{\frac{\eta^{1g}_{p_3p_2}\eta^{1g}_{p'_3p_1}}{(K_{p_3p_2}+1)\left(K_{p'_3p_1}+1\right)}}\int_{-\pi}^{\pi}\int_{R_{1n_g}}^{R_{2n_g}} e^{j2\pi\lambda^{-1}\left(\chi_{p'_3p_1,g}-\chi_{p_3p_2,g}\right)}Q_g f(\emptyset_g)d\emptyset_g d\Im_g \tag{29}$$

$$\rho^{2g}_{p_3p_2,p'_3p_1} = \sqrt{\frac{\eta^{2g}_{p_3p_2}\eta^{2g}_{p'_3p_1}}{(K_{p_3p_2}+1)\left(K_{p'_3p_1}+1\right)}}\int_{-\pi}^{\pi}\int_{-\pi}^{\pi}\int_{R_{1n_{g_1}}}^{R_{2n_{g_1}}}\int_{R_{1n_{g_2}}}^{R_{2n_{g_2}}} Q_{g_1g_2}f(\emptyset_{g_1})f(\emptyset_{g_2})$$
$$\times e^{j2\pi\lambda^{-1}\left(\chi_{p'_3p_1,g_1,g_2}-\chi_{p_3p_2,g_1,g_2}\right)}d\emptyset_{g_1}d\emptyset_{g_2}d\Im_{g_1}d\Im_{g_2} \tag{30}$$

$$\rho^{31}_{p_3p_2,p'_3p_1} = \sqrt{\frac{\eta^{31}_{p_3p_2}\eta^{31}_{p'_3p_1}}{(K_{p_3p_2}+1)\left(K_{p'_3p_1}+1\right)}}\int_{-\pi}^{\pi}\int_{-\pi}^{\pi}\int_{-\pi}^{\pi}\int_{R_{1n_1}}^{R_{2n_1}}\int_{R_{1n_2}}^{R_{2n_2}}\int_{R_{1n_3}}^{R_{2n_3}} Q_{123}$$
$$\times e^{j2\pi\lambda^{-1}\left(\chi_{p'_3p_1,1,2,3}-\chi_{p_3p_2,1,2,3}\right)}f(\emptyset_1)f(\emptyset_2)f(\emptyset_3)d\emptyset_1d\emptyset_2d\emptyset_3d\Im_1d\Im_2d\Im_3 \tag{31}$$

where $\{\emptyset_g\}_{g=1}^3 = \{\phi_1, \alpha_{2,2}, \alpha_{1,3}\}$ are the continuous expressions of the discrete expressions of angles α_{1n_1}, α_{2n_2}, α_{3n_3}, respectively, and $\varepsilon_{p_3'n_g} \approx \xi_{n_g}^B + \frac{\delta_3}{2}\cos(\beta_3 - \alpha_{1n_g})$, $\chi_{p_3'p_1,g} = \chi_{p_3'p_1,n_g}$, $\chi_{p_3p_2,g} = \chi_{p_3p_2,n_g}$, $\chi_{p_3'p_1,g_1,g_2} = \chi_{p_3'p_1,n_{g_1},n_{g_2}}$, $\chi_{p_3p_2,g_1,g_2} = \chi_{p_3p_2,n_{g_1},n_{g_2}}$, $\chi_{p_3'p_1,1,2,3} = \chi_{p_3'p_1,n_1,n_2,n_3}$, and $\chi_{p_3p_2,1,2,3} = \chi_{p_3p_2,n_1,n_2,n_3}$ with α_{1n_1}, α_{2n_2}, and α_{3n_3} being replaced by ϕ_1, $\alpha_{2,2}$, and $\alpha_{1,3}$, respectively. Parameters $f(\emptyset_g) = \exp[k_g\cos(\emptyset_g - \mu_g)]/[2\pi I_0(k_g)]$, $\{\Im_g\}_{g=1}^3 = \{\xi_{n_1}^M, \xi_{2n_2}^R, \xi_{1n_3}^B\}$, $Q_g = \frac{2\Im_{n_g}}{R_{2n_g}^2 - R_{1n_g}^2}$, $Q_{g_1g_2} = \frac{4\Im_{n_{g_1}}\Im_{n_{g_2}}}{(R_{2n_{g_1}}^2 - R_{1n_{g_1}}^2)(R_{2n_{g_2}}^2 - R_{1n_{g_2}}^2)}$, $Q_{123} = \frac{8\Im_{n_1}\Im_{n_2}\Im_{n_3}}{(R_{2n_1}^2 - R_{1n_1}^2)(R_{2n_2}^2 - R_{1n_2}^2)(R_{2n_3}^2 - R_{1n_3}^2)}$, and parameters g, g_1, and g_2 are the same as the ones in (5)–(8). Note that in (27) other correlation terms are equal to zero and thus omitted. These omitted correlation terms contain the integral of random phases ψ_{n_g}, $\psi_{n_{g_1},n_{g_2}}$, or ψ_{n_1,n_2,n_3}. Since the random phases fulfill the uniform distribution over the range of $[\pi, -\pi)$, the integral of the random phases in the range of $[\pi, -\pi)$ is equal to zero. Therefore, other correlation terms with the value of zero are omitted in (27).

Performing the substitution of (4) and (21) into (26), we can obtain the correlation function between BS-RS link and RS-MS link as

$$\rho_{p_3p_2,p_2'p_1} = \rho_{p_3p_2,p_2'p_1}^{LoS} + \sum_{g=1}^{3}(\rho_{p_3p_2,p_2'p_1}^{1g} + \rho_{p_3p_2,p_2'p_1}^{2g}) + \rho_{p_3p_2,p_2'p_1}^{31} \tag{32}$$

with

$$\rho_{p_3p_2,p_2'p_1}^{LoS} = \sqrt{\frac{K_{p_3p_2}K_{p_2'p_1}}{(K_{p_3p_2}+1)\left(K_{p_2'p_1}+1\right)}}e^{j2\pi\lambda^{-1}\left(\chi_{p_2'p_1} - \chi_{p_3p_2}\right)} \tag{33}$$

$$\rho_{p_3p_2,p_2'p_1}^{1g} = \sqrt{\frac{\eta_{p_3p_2}^{1g}\eta_{p_2'p_1}^{1g}}{(K_{p_3p_2}+1)\left(K_{p_2'p_1}+1\right)}}\int_{-\pi}^{\pi}\int_{R_{1n_g}}^{R_{2n_g}} e^{j2\pi\lambda^{-1}\left(\chi_{p_2'p_1,g} - \chi_{p_3p_2,g}\right)} Q_g f(\emptyset_g) d\emptyset_g d\Im_g \tag{34}$$

$$\rho_{p_3p_2,p_2'p_1}^{2g} = \sqrt{\frac{\eta_{p_3p_2}^{2g}\eta_{p_2'p_1}^{2g}}{(K_{p_3p_2}+1)\left(K_{p_2'p_1}+1\right)}}\int_{-\pi}^{\pi}\int_{-\pi}^{\pi}\int_{R_{1n_{g_1}}}^{R_{2n_{g_1}}}\int_{R_{1n_{g_2}}}^{R_{2n_{g_2}}} Q_{g_1g_2} f(\emptyset_{g_1}) f(\emptyset_{g_2})$$
$$\times e^{j2\pi\lambda^{-1}\left(\chi_{p_2'p_1,g_1,g_2} - \chi_{p_3p_2,g_1,g_2}\right)} d\emptyset_{g_1} d\emptyset_{g_2} d\Im_{g_1} d\Im_{g_2} \tag{35}$$

$$\rho_{p_3p_2,p_2'p_1}^{31} = \sqrt{\frac{\eta_{p_3p_2}^{31}\eta_{p_2'p_1}^{31}}{(K_{p_3p_2}+1)\left(K_{p_2'p_1}+1\right)}}\int_{-\pi}^{\pi}\int_{-\pi}^{\pi}\int_{-\pi}^{\pi}\int_{R_{1n_1}}^{R_{2n_1}}\int_{R_{1n_2}}^{R_{2n_2}}\int_{R_{1n_3}}^{R_{2n_3}} Q_{123}$$
$$\times e^{j2\pi\lambda^{-1}\left(\chi_{p_2'p_1,1,2,3} - \chi_{p_3p_2,1,2,3}\right)} f(\emptyset_1) f(\emptyset_2) f(\emptyset_3) d\emptyset_1 d\emptyset_2 d\emptyset_3 d\Im_1 d\Im_2 d\Im_3 \tag{36}$$

where $\varepsilon_{p_2'n_g} \approx \xi_{n_g}^R + \frac{\delta_2}{2}\cos(\beta_2 - \alpha_{2n_g})$, $\chi_{p_2'p_1,g} = \chi_{p_2'p_1,n_g}$, $\chi_{p_2'p_1,g_1,g_2} = \chi_{p_2'p_1,n_{g_1},n_{g_2}}$, and $\chi_{p_2'p_1,1,2,3} = \chi_{p_2'p_1,n_1,n_2,n_3}$ with α_{1n_1}, α_{2n_2}, and α_{3n_3} being replaced by ϕ_1, $\alpha_{2,2}$, and $\alpha_{1,3}$, respectively.

The substitution of (14) and (21) into (26) results in the correlation function between BS-MS link and RS-MS link as

$$\rho_{p_3p_1,p_2p_1'} = \rho^{LoS}_{p_3p_1,p_2p_1'} + \sum_{g=1}^{3}(\rho^{1g}_{p_3p_1,p_2p_1'} + \rho^{2g}_{p_3p_1,p_2p_1'}) + \rho^{31}_{p_3p_1,p_2p_1'} \tag{37}$$

with

$$\rho^{LoS}_{p_3p_1,p_2p_1'} = \sqrt{\frac{K_{p_3p_1}K_{p_2p_1'}}{(K_{p_3p_1}+1)\left(K_{p_2p_1'}+1\right)}}e^{j2\pi\lambda^{-1}\left(\chi_{p_2p_1'}-\chi_{p_3p_1}\right)} \tag{38}$$

$$\rho^{1g}_{p_3p_1,p_2p_1'} = \sqrt{\frac{\eta^{1g}_{p_3p_1}\eta^{1g}_{p_2p_1'}}{(K_{p_3p_1}+1)\left(K_{p_2p_1'}+1\right)}}\int_{-\pi}^{\pi}\int_{R_{1n_g}}^{R_{2n_g}} e^{j2\pi\lambda^{-1}\left(\chi_{p_2p_1',g}-\chi_{p_3p_1,g}\right)}Q_g f(\emptyset_g)d\emptyset_g d\Im_g, \tag{39}$$

$$\rho^{2g}_{p_3p_1,p_2p_1'} = \sqrt{\frac{\eta^{2g}_{p_3p_1}\eta^{2g}_{p_2p_1'}}{(K_{p_3p_1}+1)\left(K_{p_2p_1'}+1\right)}}\int_{-\pi}^{\pi}\int_{-\pi}^{\pi}\int_{R_{1n_{g_1}}}^{R_{2n_{g_1}}}\int_{R_{1n_{g_2}}}^{R_{2n_{g_2}}} Q_{g_1g_2}f(\emptyset_{g_1})f(\emptyset_{g_2})$$
$$\times e^{j2\pi\lambda^{-1}\left(\chi_{p_2p_1',g_1,g_2}-\chi_{p_3p_1,g_1,g_2}\right)}d\emptyset_{g_1}d\emptyset_{g_2}d\Im_{g_1}d\Im_{g_2} \tag{40}$$

$$\rho^{31}_{p_3p_1,p_2p_1'} = \sqrt{\frac{\eta^{31}_{p_3p_1}\eta^{31}_{p_2p_1'}}{(K_{p_3p_1}+1)\left(K_{p_2p_1'}+1\right)}}\int_{-\pi}^{\pi}\int_{-\pi}^{\pi}\int_{-\pi}^{\pi}\int_{R_{1n_1}}^{R_{2n_1}}\int_{R_{1n_2}}^{R_{2n_2}}\int_{R_{1n_3}}^{R_{2n_3}} Q_{123}$$
$$\times e^{j2\pi\lambda^{-1}\left(\chi_{p_2p_1',1,2,3}-\chi_{p_3p_1,1,2,3}\right)}f(\emptyset_1)f(\emptyset_2)f(\emptyset_3)d\emptyset_1d\emptyset_2d\emptyset_3d\Im_1d\Im_2d\Im_3 \tag{41}$$

where $\varepsilon_{p_1'n_g} \approx \xi^M_{n_g} + \frac{\delta_1}{2}\cos(\beta_1 - \phi_{n_g})$ with α_{1n_1}, α_{2n_2}, and α_{3n_3} being replaced by ϕ_1, $\alpha_{2,2}$, and $\alpha_{1,3}$, respectively.

For outdoor macro-cell and micro-cell BS cooperation and RS cooperation scenarios, based on the assumption $\min\{D_1, D_2, D_3\} \gg \max\{\xi^M_{n_1}, \xi^R_{n_2}, \xi^B_{n_3}\}$ correlation functions in (29)–(31), (34)–(36), and (39)–(41) can be further simplified and expressed in Appendix A. Based on the derived general spatial correlation functions, the spatial correlation functions for other scenarios can be easily obtained by following the key model parameters setting criterion explained in previous section.

V. Numerical Results and Analysis

In this section, the derived multi-link spatial correlation functions in Section IV will be numerically analyzed in detail. Without loss of generality, the spatial correlation properties between the BS-RS link and BS-MS link are chosen for further investigation. The parameters for the following numerical results are listed here or specified otherwise: $f = 2.4$GHz, $D_1 = D_3 = 100$m, $R_{1n_1} = R_{1n_2} = R_{1n_3} = 5$m, $R_{2n_1} = R_{2n_2} = R_{2n_3} = 50$m, $\delta_3 = \delta_2 = \delta_1 = 0$, $\beta_3 = 30°$, $\beta_2 = \beta_1 = 60°$, $K_{p_3p_2} = K_{p_3'p_1} = 0$, $k_1 = k_2 = k_3 = 10$, $\mu_1 = 120°$, $\mu_2 = 300°$, and $\mu_3 = 60°$.

A. Impact of Key Parameters on Multi-Link Spatial Correlation

Fig. 3 illustrates the spatial correlation properties of different components in (27) as a function of θ' and D_3. It is obvious that high spatial correlations between the BS-RS link and BS-MS link can occur at certain distances D_3 and certain values of angle θ' for different components. This again demonstrates that small scale spatial fading correlation should not be simply neglected as addressed in [27] and also highlights the importance of the work presented in this paper.

In Fig. 4, we present the spatial correlation properties of all scattered components in (27) with parameters $\delta_3 = \delta_2 = \delta_1 = 3\lambda$ and $k_1 = k_2 = k_3 = 3$. Fig. 4 clearly depicts that the spatial correlation properties vary significantly for different scattered components. More importantly, we notice that the scattered component that includes more bounced rays expresses lower spatial correlation properties. This is because with more bounced rays, the component is related to more local scattering areas and thus easier experiences higher degree of link heterogeneity, resulting in lower link similarity for this component.

Figs. 5 and 6 compare the spatial correlation properties of different scattered components for different values of environment parameters D_g, R_{1n_g}, R_{2n_g}, k_g, and μ_g with $g = 1, 2, 3$. These environment parameters determine the distance among BS, RS, and MS, and decide the size and distribution of local scattering areas. It is clear that these environment parameters significantly affect the spatial correlation properties of different scattered components. From Fig. 5, we also observe that the increase of value k_g will enhance the spatial correlation. With larger value of k_g, the scatterers in local scattering area are more concentrated and the received power mainly comes from certain direction determined by μ_g. Therefore, in this case, the spatial correlation tends to be larger, which also agrees with the conclusion in [29]. Fig. 6 also shows that the local scattering area with smaller size leads to higher spatial correlation properties. Compared to the local scattering area with larger size, the local scattering area with smaller size means the effective scatterers are more concentrated and thus results in higher spatial correlation properties. It also allows us to conclude that compared to a narrowband cooperative MIMO system, a wideband system has a high possibility to express lower spatial correlation properties as the wider the system band, the more likely the system experiences local scattering areas with larger size.

In Fig. 7, the comparison of spatial correlation properties of different scattered components for different values of antenna element spacing δ_g and antenna array tilt angles β_g with $g = 1, 2, 3$ and parameters $k_1 = k_2 = k_3 = 3$ is presented. It is shown that both antenna element spacing and antenna array tilt angle affect the spatial correlation properties of different scattered components and the increase of antenna spacing δ_g will decrease spatial correlations. However, the impact of parameters δ_g and β_g on spatial correlation properties tends to be marginal for the scattered components with more bounced rays.

B. Validation of the Proposed Cooperative MIMO GBSM

So far, based on Figs. 3–7 we have investigated in more detail the spatial correlation properties of different scattered components separately. In general, we find that the multi-link spatial correlation increases with the increase of the environment parameter k_g, with the decrease of the size of local scattering area, with the decrease of the value i for a i-bounced rays, and/or with the decrease of the antenna spacing δ_g. According to the above obtained observation and conclusions, we will investigate the spatial correlation properties of the proposed cooperative MIMO GBSM in (27) and thus validate the utility of the proposed cooperative MIMO channel model. Without loss of any generality, the outdoor macro-cell MS cooperation scenario and indoor MS cooperation scenario are chosen for further investigation. As shown in Fig. 8, three different LSD conditions are considered with parameters $\delta_3 = \delta_2 = \delta_1 = 3\lambda$, i.e., high LSD, low LSD, and mixed LSD.

For outdoor macro-cell MS cooperation scenario, as mentioned in Section III, the BS is free of scatterers and the RS actually represents the other MS, symbolled as MS2. Therefore, we have the energy-related parameters related to the local scatterers around BS to be equal to zero, i.e., $\eta^{13}_{p_3p_2} = \eta^{13}_{p'_3p_1} = \eta^{21}_{p_3p_2} = \eta^{21}_{p'_3p_1} = \eta^{22}_{p_3p_2} = \eta^{22}_{p'_3p_1} = \eta^{31}_{p_3p_2} = \eta^{31}_{p'_3p_1} = 0$, and assume $D_1 = D_3 = 1500$m and $K_{p_3p_2} = K_{p'_3p_1} = 0$ due to the large distance among BS, MS, and MS2. Considering the basic criterion of setting key model parameters expressed in Section III, we choose the other energy-related parameters as: $\eta^{11}_{p_3p_2} = \eta^{11}_{p'_3p_1} = \eta^{12}_{p_3p_2} = \eta^{12}_{p'_3p_1} = 0.05$ and $\eta^{23}_{p_3p_2} = \eta^{23}_{p'_3p_1} = 0.9$ for high LSD, and $\eta^{11}_{p_3p_2} = \eta^{11}_{p'_3p_1} = \eta^{12}_{p_3p_2} = \eta^{12}_{p'_3p_1} = 0.2$ and $\eta^{23}_{p_3p_2} = \eta^{23}_{p'_3p_1} = 0.6$ for low LSD. While for mixed LSD case, we consider the scenario that the local scattering area around MS presents low LSD and the one around MS2 shows high LSD, and thus assume the energy-related parameters as: $\eta^{11}_{p'_3p_1} = \eta^{12}_{p'_3p_1} = 0.2$, $\eta^{23}_{p'_3p_1} = 0.6$, $\eta^{11}_{p_3p_2} = \eta^{12}_{p_3p_2} = 0.1$, and $\eta^{23}_{p_3p_2} = 0.8$. In general, the higher the LSD, the more distributed and larger size the local scattering area, and thereby the smaller the value of k_g and the larger the value of $R_{2n_g} - R_{1n_g}$ ($g = 1, 2, 3$). Therefore, we have the following environment parameters as: $k_1 = k_2 = 1$, $R_{1n_1} = R_{1n_2} = 5$m, and $R_{2n_1} = R_{2n_2} = 200$m for high LSD; $k_1 = k_2 = 10$, $R_{1n_1} = R_{1n_2} = 5$m, and $R_{2n_1} = R_{2n_2} = 20$m for low LSD; and $k_1 = 10$, $k_2 = 2$, $\mu_1 = 60°$, $\mu_2 = 120°$, $R_{1n_1} = R_{1n_2} = 5$m, $R_{2n_1} = 20$m, and $R_{2n_2} = 100$m for mixed LSD.

Similarly, for indoor MS cooperation scenario, the RS actually represents the other MS, symbolled as MS2. Considering the small distance among BS, MS, and MS2, we assume $D_1 = D_3 = 50$ m. For mixed LSD case, we consider the scenario that the local scattering areas around BS and MS present low LSDs and the one around MS2 shows high LSD. The key model parameters are chosen as follows: $K_{p_3p_2} = K_{p'_3p_1} = 0.1$, $\eta^{11}_{p_3p_2} = \eta^{11}_{p'_3p_1} = \eta^{12}_{p_3p_2} = \eta^{12}_{p'_3p_1} = \eta^{13}_{p_3p_2} = \eta^{13}_{p'_3p_1} = 0.05$, $\eta^{21}_{p_3p_2} = \eta^{21}_{p'_3p_1} =$

$\eta^{22}_{p_3p_2} = \eta^{22}_{p'_3p_1} = \eta^{23}_{p_3p_2} = \eta^{23}_{p'_3p_1} = 0.2$, and $\eta^{31}_{p_3p_2} = \eta^{31}_{p'_3p_1} = 0.25$ for high LSD; $K_{p_3p_2} = K_{p'_3p_1} = 3$, $\eta^{11}_{p_3p_2} = \eta^{11}_{p'_3p_1} = \eta^{12}_{p_3p_2} = \eta^{12}_{p'_3p_1} = \eta^{13}_{p_3p_2} = \eta^{13}_{p'_3p_1} = 0.3$, and $\eta^{21}_{p_3p_2} = \eta^{21}_{p'_3p_1} = \eta^{22}_{p_3p_2} = \eta^{22}_{p'_3p_1} = \eta^{23}_{p_3p_2} = \eta^{23}_{p'_3p_1} = \eta^{31}_{p_3p_2} = \eta^{31}_{p'_3p_1} = 0.025$ for low LSD; and $K_{p_3p_2} = 0.5$, $K_{p'_3p_1} = 2.5$, $\eta^{11}_{p'_3p_1} = \eta^{12}_{p'_3p_1} = \eta^{13}_{p'_3p_1} = 0.25$, $\eta^{21}_{p'_3p_1} = 0.1$, $\eta^{22}_{p'_3p_1} = \eta^{23}_{p'_3p_1} = \eta^{31}_{p'_3p_1} = 0.05$, $\eta^{11}_{p_3p_2} = \eta^{12}_{p_3p_2} = \eta^{13}_{p_3p_2} = 0.05$, $\eta^{21}_{p_3p_2} = \eta^{23}_{p_3p_2} = 0.3$, $\eta^{22}_{p_3p_2} = 0.1$, and $\eta^{31}_{p_3p_2} = 0.15$ for mixed LSD. The following environment parameters are selected as: $k_1 = k_2 = k_3 = 1$, $R_{1n_1} = R_{1n_2} = R_{1n_3} = 2$m, and $R_{2n_1} = R_{2n_2} = R_{2n_3} = 25$m for high LSD; $k_1 = k_2 = k_3 = 10$, $R_{1n_1} = R_{1n_2} = R_{1n_3} = 2$m, and $R_{2n_1} = R_{2n_2} = R_{2n_3} = 8$m for low LSD; and $k_1 = 6$, $k_2 = 2$, $k_3 = 15$, $\mu_1 = 60°$, $\mu_2 = 120°$, $\mu_3 = 240°$, $R_{1n_1} = R_{1n_2} = R_{1n_3} = 2$m, $R_{2n_1} = 12$m, $R_{2n_2} = 20$m, and $R_{2n_3} = 5$m for mixed LSD.

Fig. 8 clearly shows that the LSD significantly affects the spatial correlation properties. It is observed that the higher the LSD, the lower the spatial correlation properties. This is because that with a higher LSD, the local scattering area is more distributed and presents larger size, resulting in the received power comes from many different directions. Fig. 8 also illustrates that the indoor MS cooperation scenario has larger spatial correlation properties than the outdoor macro-cell MS cooperation scenario. This is basically resulted from the appearance of a LoS component in the indoor MS cooperation scenario due to the smaller distance among BS, MS, and MS2. Therefore, we can conclude that a high multi-link spatial correlation normally appears in a scenario with lower LSDs and LoS components. More importantly, from the observation in Fig. 4 and based on the constraints of the energy-related parameters for cooperative scenarios with different LSDs, we know that with a higher LSD, the multi-bounced components bear more energy than single-bounced components and thus the corresponding cooperative environment has a higher possibility to reveal a high degree of link heterogeneity, i.e., a low degree of environment similarity. Therefore, the above conclusion based on Fig. 8 is consistent with our intuition that a low degree of environment similarity results in low multi-link spatial correlations.

VI. Conclusions

This paper has proposed a novel unified cooperative MIMO channel model framework, from which a novel GBSM has been further derived. The proposed multiple-ring GBSM is sufficiently generic and adaptable to a wide variety of cooperative MIMO propagation scenarios. More importantly, the proposed GBSM is the first model that is capable of investigating the impact of LSD on channel statistics. From the proposed GBSM, the multi-link spatial correlations have been derived and numerically evaluated. Numerical results have shown that the antenna element spacings, environment parameters, and LSD have great impacts on multi-link spatial correlation properties. It has also been demonstrated that a high

multi-link spatial correlation may exist if a cooperative communication system has a relatively narrow bandwidth and the underlying propagation environments have low LSDs and LoS components.

APPENDIX

A. THE REDUCED EXPRESSIONS OF SPATIAL CORRELATION

For outdoor macro-cell and micro-cell BS cooperation and relay cooperation scenarios, the assumption $\min\{D_1, D_2, D_3\} \gg \max\{\xi^M_{n_1}, \xi^R_{n_2}, \xi^B_{n_3}\}$ is applicable. In this case, by using trigonometric transformations, the equality $\int_{-\pi}^{\pi} e^{a\sin c + b\cos c} dc = 2\pi I_0\left(\sqrt{a^2+b^2}\right)$ [35], and the results in [32], the spatial correlation between BS-RS link and BS-MS link in (29)–(31) can be reduced as

$$\rho^{1g}_{p_3p_2,p'_3p_1} = \sqrt{\frac{\eta^{1g}_{p_3p_2}\eta^{1g}_{p'_3p_1}}{I_0\{k_g\}\left(K_{p_3p_2}+1\right)\left(K_{p'_3p_1}+1\right)}} e^{jC^{11}} \int_{R_{1n_g}}^{R_{2n_g}} e^{jE^{11}} I_0\{\sqrt{(A^{1g})^2+(B^{1g})^2}\} Q_g d\Im_g \quad (42)$$

$$\rho^{2g}_{p_3p_2,p'_3p_1} = \sqrt{\frac{\eta^{2g}_{p_3p_2}\eta^{2g}_{p'_3p_1}}{I_0\{k_{g_1}\}I_0\{k_{g_2}\}\left(K_{p_3p_2}+1\right)\left(K_{p'_3p_1}+1\right)}} e^{jC^{2g}}$$
$$\times \int_{R_{1n_{g_1}}}^{R_{2n_{g_1}}} \int_{R_{1n_{g_2}}}^{R_{2n_{g_2}}} e^{jE^{2g}} I_0\{\sqrt{(A^{2g}_1)^2+(B^{2g}_1)^2}\} I_0\{\sqrt{(A^{2g}_2)^2+(B^{2g}_2)^2}\} Q_{g_1g_2} d\Im_{g_1} d\Im_{g_2} \quad (43)$$

$$\rho^{31}_{p_3p_2,p'_3p_1} = \sqrt{\frac{\eta^{31}_{p_3p_2}\eta^{31}_{p'_3p_1}}{I_0\{k_1\}I_0\{k_2\}I_0\{k_3\}\left(K_{p_3p_2}+1\right)\left(K_{p'_3p_1}+1\right)}} e^{jC^{31}}$$
$$\times \int_{R_{1n_1}}^{R_{2n_1}} \int_{R_{1n_2}}^{R_{2n_2}} \int_{R_{1n_3}}^{R_{2n_3}} e^{jE^{31}} I_0\{\sqrt{(A^{31}_M)^2+(B^{31}_M)^2}\}$$
$$\times I_0\{\sqrt{(A^{31}_R)^2+(B^{31}_R)^2}\} I_0\{\sqrt{(A^{31}_B)^2+(B^{31}_B)^2}\} Q_{123} d\Im_1 d\Im_2 d\Im_3 \quad (44)$$

where $C^{11} = C^{11}_p - 2\pi\lambda^{-1}\delta_3\cos\beta_3$ with $C^{11}_P = -2\pi\lambda^{-1}[D_2 + \frac{\delta_2}{2}\cos(\beta_2+\theta)]$, $E^{11} = E^{22} = 2\pi\lambda^{-1}\xi^M_{n_1}$, $A^{11} = A^{22}_1 - j2\pi\lambda^{-1}\delta_3\sin\beta_3\frac{\xi^M_{n_1}}{D_1}$, $B^{11} = B^{22}_1 = -j2\pi\lambda^{-1}[\frac{\delta_1}{2}\cos\beta_1 - \xi^M_{n_1} + \frac{\delta_2\xi^M_{n_1}}{2D_2}\sin(\beta_2+\theta)\sin\theta] + k_1\cos\mu_1$ $C^{12} = C^{12}_P + 2\pi\lambda^{-1}\delta_3\cos(\beta_3-\theta')]$ with $C^{22}_P = 2\pi\lambda^{-1}[D_2 + \frac{\delta_1}{2}\cos(\beta_1+\theta)]$, $E^{12} = E^{21} = -2\pi\lambda^{-1}\xi^R_{n_2}$, $A^{12} = A^{21}_1 - j2\pi\lambda^{-1}\delta_3\sin(\beta_3-\theta')\frac{\xi^R_{n_2}}{D_3}\cos\theta'$, $B^{12} = B^{21}_1 + j2\pi\lambda^{-1}\delta_3\sin(\beta_3-\theta')\frac{\xi^R_{n_2}}{D_3}\sin\theta'$, $C^{13} = 2\pi\lambda^{-1}[\frac{\delta_1}{2}\cos\beta_1 - \frac{\delta_2}{2}\cos(\theta'-\beta_2)] - C^{31}$, $E^{13} = E^{21} = E^{22} = 0$, $A^{13} = A^{31}_B + j2\pi\lambda^{-1}[\xi^B_{n_3}\sin\theta' - \frac{\delta_1\xi^B_{n_3}}{2D_1}\sin\beta_1 + \frac{\delta_2\xi^B_{n_3}}{2D_3}\sin(\theta'-\beta_2)\cos\theta']$, $B^{13} = B^{31}_B + j2\pi\lambda^{-1}[\xi^B_{n_3}\cos\theta' - \xi^B_{n_3} - \frac{\delta_2\xi^B_{n_3}}{2D_3}\sin(\theta'-\beta_2)\sin\theta']$, $C^{21} = C^{12}_P - 2\pi\lambda^{-1}\delta_1\cos\beta_1$, $A^{21}_1 = j2\pi\lambda^{-1}[\xi^R_{n_2}\sin\theta + \frac{\delta_2}{2}\sin\beta_2 + \frac{\delta_1\xi^R_{n_2}}{2D_2}\sin(\beta_1+\theta)\cos\theta] + k_2\sin\mu_2$, $B^{21}_1 = j2\pi\lambda^{-1}[\frac{\delta_2}{2}\cos\beta_2 - \xi^R_{n_2}\cos\theta + \frac{\delta_1\xi^R_{n_2}}{2D_2}\sin(\beta_1+\theta)\sin\theta] + k_2\cos\mu_2$, $A^{21}_2 = A^{22}_2 = j2\pi\lambda^{-1}\delta_1\sin\beta_1\frac{\xi^B_{n_3}}{D_1} + k_3\sin\mu_3$, $B^{21}_2 = B^{22}_2 = k_3\cos\mu_3$, $C^{22} = C^{11}_P - 2\pi\lambda^{-1}\delta_1\cos\beta_1$, $A^{22}_1 = -j2\pi\lambda^{-1}[\frac{\delta_1}{2}\sin\beta_1 + \frac{\delta_2\xi^M_{n_1}}{2D_2}\sin(\beta_2+\theta)\cos\theta] + k_1\sin\mu_1$, $C^{23} = c^{31} + 2\pi\lambda^{-1}[\frac{\delta_3}{2}\cos\beta_3 + \frac{\delta_3}{2}\cos(\beta_3-\theta')]$, $E^{23} = E^{11} + E^{12}$, $A^{23}_1 = A^{31}_M + j2\pi\lambda^{-1}\frac{\delta_3}{2}\sin\beta_3\frac{\xi^M_{n_1}}{D_1}$, $B^{23}_1 = B^{31}_M - j2\pi\lambda^{-1}\xi^M_{n_1}$, $A^{23}_2 = A^{12} - j2\pi\lambda^{-1}\frac{\delta_1\xi^R_{n_2}}{2D_2}\sin(\beta_1+\theta)\cos\theta$, $B^{23}_2 = A^{12} - j2\pi\lambda^{-1}\frac{\delta_1\xi^R_{n_2}}{2D_2}\sin(\beta_1+\theta)\sin\theta$, $C^{31} = 2\pi\lambda^{-1}[D_3 - D_1]$,

$E^{31}=E^{11}-E^{12}$, $A^{31}_{M(R)}=\mp j2\pi\lambda^{-1}\frac{\delta_{3(2)}}{2}\sin\beta_{3(2)}+k_{n_{1(2)}}\sin\mu_{n_{1(2)}}$, $B^{31}_{M(R)}=\mp j2\pi\lambda^{-1}\frac{\delta_{3(2)}}{2}\cos\beta_{3(2)}+k_{n_{1(2)}}\cos\mu_{n_{1(2)}}$, $A^{31}_{B}=j2\pi\lambda^{-1}\delta_3\sin\beta_3+k_3\sin\mu_3$, $B^{31}_{B}=j2\pi\lambda^{-1}\delta_3\cos\beta_3+k_3\cos\mu_3$.

Similarly, we can reduced the spatial correlation between BS-RS link and RS-MS link in (34)–(36) as

$$\rho^{1g}_{p_3p_2,p'_2p_1}=\sqrt{\frac{\eta^{1g}_{p_3p_2}\eta^{1g}_{p'_2p_1}}{I_0\{k_g\}\left(K_{p_3p_2}+1\right)\left(K_{p'_2p_1}+1\right)}}e^{j\widetilde{C}^{11}}\int_{R_{1n_g}}^{R_{2n_g}}e^{j\widetilde{E}^{11}}I_0\{\sqrt{(\widetilde{A}^{1g})^2+(\widetilde{B}^{1g})^2}\}Q_g d\Im_g \quad (45)$$

$$\rho^{2g}_{p_3p_2,p'_2p_1}=\sqrt{\frac{\eta^{2g}_{p_3p_2}\eta^{2g}_{p'_2p_1}}{I_0\{k_{g_1}\}I_0\{k_{g_2}\}\left(K_{p_3p_2}+1\right)\left(K_{p'_2p_1}+1\right)}}e^{j\widetilde{C}^{21}}$$
$$\times\int_{R_{1n_{g_1}}}^{R_{2n_{g_1}}}\int_{R_{1n_{g_2}}}^{R_{2n_{g_2}}}e^{j\widetilde{E}^{21}}I_0\{\sqrt{(\widetilde{A}^{2g}_1)^2+(\widetilde{B}^{2g}_1)^2}\}I_0\{\sqrt{(\widetilde{A}^{2g}_2)^2+(\widetilde{B}^{2g}_2)^2}\}Q_{g_1g_2}d\Im_{g_1}d\Im_{g_2} \quad (46)$$

$$\rho^{31}_{p_3p_2,p'_2p_1}=\sqrt{\frac{\eta^{31}_{p_3p_2}\eta^{31}_{p'_2p_1}}{I_0\{k_1\}I_0\{k_2\}I_0\{k_3\}\left(K_{p_3p_2}+1\right)\left(K_{p'_2p_1}+1\right)}}e^{j\widetilde{C}^{31}}$$
$$\times\int_{R_{1n_1}}^{R_{2n_1}}\int_{R_{1n_2}}^{R_{2n_2}}\int_{R_{1n_3}}^{R_{2n_3}}e^{jE^{31}}I_0\{\sqrt{(\widetilde{A}^{31}_M)^2+(\widetilde{B}^{31}_M)^2}\}$$
$$\times I_0\{\sqrt{(\widetilde{A}^{31}_R)^2+(\widetilde{B}^{31}_R)^2}\}I_0\{\sqrt{(\widetilde{A}^{31}_B)^2+(\widetilde{B}^{31}_B)^2}\}Q_{123}d\Im_1d\Im_2d\Im_3 \quad (47)$$

where $\widetilde{C}^{11}=\widetilde{C}^{11}_P-2\pi\lambda^{-1}\delta_2\cos(\beta_2+\theta)$ with $\widetilde{C}^{11}_P=-2\pi\lambda^{-1}[D_1-\frac{\delta_3}{2}\cos\beta_3]$, $\widetilde{E}^{11}=\widetilde{E}^{22}=2\pi\lambda^{-1}\xi^M_{n_1}$, $\widetilde{A}^{11}=\widetilde{A}^{22}_1-j2\pi\lambda^{-1}\frac{\delta_2\xi^M_{n_1}}{D_2}\sin(\beta_2+\theta)\cos\theta$, $\widetilde{B}^{11}=\widetilde{B}^{22}_1-j2\pi\lambda^{-1}\frac{\delta_2\xi^M_{n_1}}{D_2}\sin(\beta_2+\theta)\sin\theta$, $\widetilde{C}^{12}=2\pi\lambda^{-1}[D_2+\frac{\delta_1}{2}\cos(\beta_1+\theta)+\frac{\delta_3}{2}\cos(\beta_3-\theta')]-\widetilde{C}^{31}$, $\widetilde{E}^{12}=0$, $\widetilde{A}^{12}=\widetilde{A}^{21}_2+j2\pi\lambda^{-1}[\xi^R_{n_2}\sin\theta+\frac{\delta_1\xi^R_{n_2}}{2D_2}\sin(\beta_1+\theta)\cos\theta-\xi^R_{n_2}\sin\theta'-\frac{\delta_3}{2}\sin(\beta_3-\theta')\frac{\xi^R_{n_2}}{D_3}\cos\theta']$, $\widetilde{B}^{12}=\widetilde{B}^{31}_R+j2\pi\lambda^{-1}[\xi^R_{n_2}\cos\theta+\frac{\delta_1\xi^R_{n_2}}{2D_2}\sin(\beta_1+\theta)\sin\theta-\xi^R_{n_2}\cos\theta'+\frac{\delta_3}{2}\sin(\beta_3-\theta')\frac{\xi^R_{n_2}}{D_3}\sin\theta']$, $\widetilde{C}^{13}=\widetilde{C}^{21}_1-2\pi\lambda^{-1}\delta_2\cos(\theta'-\beta_2)$, $\widetilde{E}^{13}=\widetilde{E}^{21}_1=-2\pi\lambda^{-1}\xi^B_{n_3}$, $\widetilde{A}^{13}=\widetilde{A}^{21}_1+j2\pi\lambda^{-1}\frac{\delta_2\xi^B_{n_3}}{D_3}\sin(\theta'-\beta_2)\cos\theta'$, $\widetilde{B}^{13}=\widetilde{B}^{21}_1-j2\pi\lambda^{-1}\frac{\delta_2\xi^B_{n_3}}{D_3}\sin(\theta'-\beta_2)\sin\theta'$, $\widetilde{C}^{21}=2\pi\lambda^{-1}[D_1+\frac{\delta_1}{2}\cos\beta_1]$, $\widetilde{A}^{21}_1=j2\pi\lambda^{-1}[-\frac{\delta_1\xi^B_{n_3}}{2D_1}\sin\beta_1-\frac{\delta_3}{2}\sin\beta_3]+k_3\sin\mu_3$, $\widetilde{B}^{21}_1=j2\pi\lambda^{-1}[-\xi^B_{n_3}-\frac{\delta_3}{2}\cos\beta_3]+k_3\cos\mu_3$, $\widetilde{A}^{21}_2=\widetilde{A}^{31}_R=j2\pi\lambda^{-1}\delta_2\sin\beta_2+k_2\sin\mu_2$, $\widetilde{B}^{21}_2=\widetilde{B}^{31}_R=j2\pi\lambda^{-1}\delta_2\cos\beta_2+k_2\cos\mu_2$, $\widetilde{C}^{22}=\widetilde{C}^{11}_P-2\pi\lambda^{-1}\cos(\theta'-\beta_2)$, $\widetilde{A}^{22}_1=-j2\pi\lambda^{-1}[\frac{\delta_1}{2}\sin\beta_1+-\frac{\delta_3}{2}\sin\beta_3\frac{\xi^M_{n_1}}{D_1}]+k_1\sin\mu_1$, $\widetilde{B}^{22}_1=-j2\pi\lambda^{-1}[\frac{\delta_1}{2}\cos\beta_1+\xi^M_{n_1}]+k_1\cos\mu_1$, $\widetilde{A}^{22}_2=j2\pi\lambda^{-1}\sin(\theta'-\beta_2)\frac{\xi^B_{n_3}}{D_3}\cos\theta+k_3\sin\mu_3$, $\widetilde{B}^{22}_2=-j2\pi\lambda^{-1}\sin(\theta'-\beta_2)\frac{\xi^B_{n_3}}{D_3}\sin\theta+k_3\cos\mu_3$, $\widetilde{C}^{31}=2\pi\lambda^{-1}[D_3-D_2]$, $\widetilde{E}^{31}=\widetilde{E}^{11}-\widetilde{E}^{13}$, $\widetilde{A}^{31}_{M(B)}=\mp j2\pi\lambda^{-1}\frac{\delta_{3(1)}}{2}\sin\beta_{3(1)}+k_{n_{1(3)}}\sin\mu_{n_{1(3)}}$, $\widetilde{B}^{31}_{M(B)}=\mp j2\pi\lambda^{-1}\frac{\delta_{3(1)}}{2}\cos\beta_{3(1)}+k_{n_{1(3)}}\cos\mu_{n_{1(3)}}$.

For BS-MS link and RS-MS link, the spatial correlation between them shown in (39)–(41) can be reduced as

$$\rho^{1g}_{p_3p_1,p_2p_1'}=\sqrt{\frac{\eta^{1g}_{p_3p_1}\eta^{1g}_{p_2p_1'}}{I_0\{k_g\}\left(K_{p_3p_1}+1\right)\left(K_{p_2p_1'}+1\right)}}e^{j\widehat{C}^{11}}\int_{R_{1n_g}}^{R_{2n_g}}e^{j\widehat{E}^{11}}I_0\{\sqrt{(\widehat{A}^{1g})^2+(\widehat{B}^{1g})^2}\}Q_g d\Im_g \quad (48)$$

$$\rho^{2g}_{p_3p_1,p_2p_1'}=\sqrt{\frac{\eta^{2g}_{p_3p_1}\eta^{2g}_{p_2p_1'}}{I_0\{k_{g_1}\}I_0\{k_{g_2}\}\left(K_{p_3p_1}+1\right)\left(K_{p_2p_1'}+1\right)}}e^{j\widehat{C}^{2g}}$$
$$\times\int_{R_{1n_{g1}}}^{R_{2n_{g1}}}\int_{R_{1n_{g2}}}^{R_{2n_{g2}}}e^{j\widehat{E}^{2g}}I_0\{\sqrt{(\widehat{A}^{2g}_1)^2+(\widehat{B}^{2g}_1)^2}\}I_0\{\sqrt{(\widehat{A}^{2g}_2)^2+(\widehat{B}^{2g}_2)^2}\}Q_{g_1g_2}d\Im_{g_1}d\Im_{g_2} \quad (49)$$

$$\rho^{31}_{p_3p_1,p_2p_1'}=\sqrt{\frac{\eta^{31}_{p_3p_1}\eta^{31}_{p_2p_1'}}{I_0\{k_1\}I_0\{k_2\}I_0\{k_3\}\left(K_{p_3p_1}+1\right)\left(K_{p_2p_1'}+1\right)}}e^{j\widehat{C}^{31}}$$
$$\times\int_{R_{1n_1}}^{R_{2n_1}}\int_{R_{1n_2}}^{R_{2n_2}}\int_{R_{1n_3}}^{R_{2n_3}}e^{jE^{31}}I_0\{\sqrt{(\widehat{A}^{31}_M)^2+(\widehat{B}^{31}_M)^2}\}$$
$$\times I_0\{\sqrt{(\widehat{A}^{31}_R)^2+(\widehat{B}^{31}_R)^2}\}I_0\{\sqrt{(\widehat{A}^{31}_B)^2+(\widehat{B}^{31}_B)^2}\}Q_{123}d\Im_1d\Im_2d\Im_3 \quad (50)$$

where $\widehat{C}^{11}=2\pi\lambda^{-1}[D_2+\frac{\delta_2}{2}\cos(\beta_2+\theta)-D_1+\frac{\delta_3}{2}\cos\beta_3]$, $\widehat{E}^{11}=0$, $\widehat{A}^{11}=\widehat{A}^{22}_1+j2\pi\lambda^{-1}[\frac{\delta_2\xi^M_{n_1}}{2D_2}\sin(\beta_2+\theta)\cos\theta+\frac{\delta_3}{2}\sin\beta_3\frac{\xi^M_{n_1}}{D_1}]$, $\widehat{B}^{11}=\widehat{B}^{22}_1+j2\pi\lambda^{-1}[-2\xi^M_{n_1}+\frac{\delta_2\xi^M_{n_1}}{2D_2}\sin(\beta_2+\theta)\sin\theta]$, $\widehat{C}^{12}=\widehat{C}^{23}-2\pi\lambda^{-1}\delta_1\cos(\beta_1+\theta)$, $\widehat{E}^{12}=\widehat{E}^{23}=2\pi\lambda^{-1}\xi^R_{n_2}$, $\widehat{A}^{12}=\widehat{A}^{23}_2-j2\pi\lambda^{-1}\frac{\delta_1\xi^R_{n_2}}{D_2}\sin(\beta_1+\theta)\cos\theta$, $\widehat{B}^{12}=\widehat{B}^{23}_2-j2\pi\lambda^{-1}\frac{\delta_1\xi^R_{n_2}}{D_2}\sin(\beta_1+\theta)\sin\theta$, $\widehat{C}^{13}=\widehat{C}^{22}-2\pi\lambda^{-1}\delta_1\cos\beta_1$, $\widehat{E}^{13}=\widehat{E}^{22}=-2\pi\lambda^{-1}\xi^B_{n_3}$, $\widehat{A}^{13}=\widehat{A}^{22}_2+j2\pi\lambda^{-1}\frac{\delta_1\xi^B_{n_3}}{D_1}\sin\beta_1$, $\widehat{B}^{13}=\widehat{B}^{22}_2=-j2\pi\lambda^{-1}[\xi^B_{n_3}\cos\theta'-\frac{\delta_2\xi^B_{n_3}}{2D_3}\sin(\theta'-\beta_2)\sin\theta'+\frac{\delta_3}{2}\cos\beta_3]+k_3\cos\mu_3$, $\widehat{C}^{21}=\widehat{C}^{31}-2\pi\lambda^{-1}\frac{\delta_1}{2}(\cos\beta_1+\cos(\beta_1+\theta))$, $\widehat{E}^{21}=\widehat{E}^{31}=\widehat{E}^{12}+\widehat{E}^{13}$, $\widehat{A}^{21}_1=-j2\pi\lambda^{-1}[-\xi^R_{n_2}\sin\theta+\frac{\delta_1\xi^R_{n_2}}{2D_2}\sin(\beta_1+\theta)\cos\theta+\frac{\delta_2}{2}\sin\beta_2]+k_2\sin\mu_2$, $\widehat{B}^{21}_1=-j2\pi\lambda^{-1}[-\xi^R_{n_2}\cos\theta+\frac{\delta_1\xi^R_{n_2}}{2D_2}\sin(\beta_1+\theta)\sin\theta+\frac{\delta_2}{2}\cos\beta_2]+k_2\cos\mu_2$, $\widehat{A}^{21}_2=j2\pi\lambda^{-1}[\frac{\delta_1\xi^B_{n_3}}{2D_1}\sin\beta_1+\frac{\delta_3}{2}\sin\beta_3]+k_3\sin\mu_3$, $\widehat{B}^{21}_2=j2\pi\lambda^{-1}[-\xi^B_{n_3}+\frac{\delta_3}{2}\cos\beta_3]+k_3\cos\mu_3$, $\widehat{C}^{22}=2\pi\lambda^{-1}[D_3+\frac{\delta_2}{2}\cos(\theta'-\beta_2)]$, $\widehat{A}^{22}_1=\widehat{A}^{23}_1=\widehat{A}^{31}_M=j2\pi\lambda^{-1}\delta_1\sin\beta_1+k_1\sin\mu_1$, $\widehat{B}^{22}_1=\widehat{B}^{23}_1=\widehat{B}^{31}_M=j2\pi\lambda^{-1}\delta_1\cos\beta_1+k_1\cos\mu_1$, $\widehat{A}^{22}_2=-j2\pi\lambda^{-1}[\frac{\delta_3}{2}\sin\beta_3+\xi^B_{n_3}\sin\theta'+\frac{\delta_2\xi^B_{n_3}}{2D_3}\sin(\theta'-\beta_2)\cos\theta']+k_3\sin\mu_3$, $\widehat{C}^{23}=2\pi\lambda^{-1}[-D_3+\frac{\delta_3}{2}\cos(\beta_3-\theta')]$, $\widehat{A}^{23}_2=-j2\pi\lambda^{-1}[\frac{\delta_2}{2}\sin\beta_2+\xi^R_{n_2}\sin\theta'+\frac{\delta_3}{2}\sin(\beta_3-\theta')\frac{\xi^R_{n_2}}{D_3}\cos\theta']+k_2\sin\mu_2$, $\widehat{B}^{23}_2=-j2\pi\lambda^{-1}[\frac{\delta_2}{2}\cos\beta_2+\xi^R_{n_2}\cos\theta'-\frac{\delta_3}{2}\sin(\beta_3-\theta')\frac{\xi^R_{n_2}}{D_3}\sin\theta']+k_2\cos\mu_2$, $\widehat{C}^{31}=2\pi\lambda^{-1}[D_1-D_2]$, $\widehat{A}^{31}_{R(B)}=-j2\pi\lambda^{-1}\frac{\delta_{2(1)}}{2}\sin\beta_{2(1)}+k_{n_{2(3)}}\sin\mu_{n_{2(3)}}$, $\widehat{B}^{31}_{R(B)}=-j2\pi\lambda^{-1}\frac{\delta_{2(1)}}{2}\cos\beta_{2(1)}+k_{n_{2(3)}}\cos\mu_{n_{2(3)}}$.

REFERENCES

[1] IEEE 802.11n-2009–Amendment 5, "Enhancements for Higher Throughput," Tech. Rep., Oct. 2009.

[2] K. Fazel and S. Kaiser, *Multi-Carrier and Spread Spectrum Systems: From OFDM and MC-CDMA to LTE and WiMAX*, 2nd ed. John Wiley & Sons, 2008.

[3] G. J. Foschini, "Layered space-time architecture for wireless communication in a fading environment when using multiple antennas," *Bell Labs. Tech. J.*, vol. 1, no. 2, pp. 41–59, Summer 1996.

[4] G. J. Foschini and M. J. Gans, "On limits of wireless communications in a fading environment when using multiple antennas," *Wireless Personal Commun.*, vol. 6, no. 2, pp. 311–335, 1998.

[5] A. Sendonaris, E. Erkip, and B. Aazhang, "User cooperation diversity–Part I: System description," *IEEE Trans. Commun.*, vol. 51, no. 11, pp. 1927–1938, Nov. 2003.

[6] A. Sendonaris, E. Erkip, and B. Aazhang, ”User cooperation diversity–Part II: Implementation aspects and performance analysis,” *IEEE Trans. Commun.*, vol. 51, no. 11, pp. 1939–1948, Nov. 2003.

[7] V. Mahinthan, J. W. Mark, and X. Shen, ”A cooperative diversity scheme based on quadrature signaling,” *IEEE Trans. Wireless Commun.*, vol. 6, no. 1, pp. 41–45, Jan. 2007.

[8] M. Mahinthan, X. Shen, and K. Naik, ”Cooperative fair scheduling for the downlink of CDMA cellular networks,” *IEEE Trans. Veh. Technol.*, vol. 56, no. 4, pp. 1749–1760, Jul. 2007.

[9] V. Mahinthan, J. W. Mark, and X. Shen, ”Performance analysis and power allocation for M-QAM cooperative diversity systems,” *IEEE Trans. Wireless Commun.*, vol. 9, no. 3, pp. 1237–1247, Mar. 2010.

[10] Z. Han, X. Zhang, and H. V. Poor, ”High performance cooperative transmission protocols based on multiuser detection and network coding,” *IEEE Trans. Wireless Commun.*, vol. 8, no. 5, pp. 41–45, May 2009.

[11] M. R. Bhatnagar and A. Hjøungnes, ”Improved interference cancellation scheme for two-user detection of Alamouti code,” *IEEE Trans. Signal Process.*, vol. 58, no. 8, pp. 4459–4465, Aug. 2010.

[12] Q. Zhang, J. Jia, and J. Zhang, ”Cooperative relay to improve diversity in cognitive radio networks,” *IEEE Commun. Mag.*, vol. 47, no. 2, pp. 111–117, Feb. 2009.

[13] C. L. Robinson, D. Caveney, L. Caminiti, G. Baliga, K. Laberteaux, and P. R. Kumar, ”Efficient message composition and coding for cooperative vehicular safety applications,” *IEEE Trans. Veh. Technol.*, vol. 56, no. 6, pp. 3244–3255, Nov. 2007.

[14] L. Dong, Z. Han, A. P. Petropulu, and H. V. Poor, ”Improving wireless physical layer security via cooperating relays,” *IEEE Trans. Signal Process.*, vol. 58, no. 3, pp. 1875–1888, Mar. 2010.

[15] C.-X. Wang, X. Cheng, and D. I. Laurenson, ”Vehicle-to-vehicle channel modeling and measurements: recent advances and future challenges”, *IEEE Commun. Mag.*, vol. 47, no. 11, pp. 96–103, Nov. 2009.

[16] J. Medbo, J. E. Berg, and F. Harrysson, ”Temporal radio channel variations with stationary terminal,” *Proc. VTC’04-Fall*, California, USA, Sept. 2004, pp. 91–95.

[17] J. Karedal, A. Johansson, F. Tufvesson, and A. Molisch, ”A measurement-based fading model for wireless personal area networks,” *IEEE Trans. Wireless Commun.*, vol. 7, no. 11, pp. 4575–4585, Nov. 2008.

[18] P. Almers, K. Haneda, J. Koivunen, V. M. Kolmonen, A. Molisch, A. Richter, J. Salmi, F. Fufvesson, and P. Vainikainen, ”A dynamic multi-link MIMO measurement system for 5.3 GHz,” *Proc. 29th URSI Gen. Assem.*, Chicago, USA, Aug. 2008.

[19] P. Soma, D. Baum, V. Erceg, R. Krishnamoorthy, and A. Paulraj, ”Analysis and modeling of multiple-input multiple-output radio channels based on outdoor measurements conducted at 2.5 GHz for fixed BWA applications,” *Proc. ICC’02*, New York, USA, May 2002, pp. 272–276.

[20] L. Ahumada, R. Feick, R. Valenzuela, and C. Morales, ”Measurement and characterization of the temporal behavior of fixed wireless links,” *IEEE Trans. Veh. Technol.*, vol. 54, no. 6, pp. 1913–1922, Nov. 2005.

[21] F. Kaltenberger, M. Kountouris, D. Gesbert, and R. Knopp, ”Correlation and capacity of measured multi-user MIMO channels,” *Proc. PIMRC’08*, Cannes, France, Sept. 2008, pp. 1–5.

[22] L. Jiang, L. Thiele, and V. Jungnickel, ”Modeling and measurement of MIMO relay channels,” *Proc. VTC’08-Spring*, Singapore, May 2008, pp. 419–423.

[23] J. Zhang, D. Dong, X. Nie, Y. Liang, C. Huang, G. Liu, and W. Dong, ”Propagation characteristics of wideband relay channels in Urban environment,” *Proc. Wirkshop on Broadband MIMO Channel Measurement and Modeling*, Beijing, China, Aug. 2009, pp. 1–5.

[24] 3GPP TR 25.996, ”Spatial channel model for multiple input multiple output (MIMO) simulations (Rel. 6),” Sept. 2003.

[25] P. Kyosti *et al.*, ”WINNER II channel models,” IST-WINNER II D1.1.2, Nov. 2007.

[26] G. Senarth *et al.*, ”Multi-hop relay system evaluation methodology (Channel model and performance metric),” IEEE 802.16j-06/013r3, Feb. 2007.

[27] C.-X. Wang, X. Hong, X. Ge, X. Cheng, G. Zhang, and J. Thompson, ”Cooperative MIMO channel models: A survey,” *IEEE Commun. Mag.*, vol. 48, no. 2, pp. 80–87, Feb. 2010.

[28] C. Oestges, N. Czink, B. Bandemer, P. Castiglione, F. Kaltenberger, and A. Paulraj, ”Experimental characterization and modeling of outdoor-to-indoor and indoor-to-indoor distributed channels,” *IEEE Trans. Veh. Technol.*, vol. 59, no. 3, pp. 2253–2265, Jun. 2010.

[29] W. Xu, S. A. Zekavat, and H. Tong, ”A novel spatially correlated multiuser MIMO channel modeling: Impact of surface roughness,” *IEEE Trans. Antennas Propag.*, vol. 57, no. 8, pp. 2429–2438, Aug. 2009.

[30] X. Yin, ”Spatial cross-correlation of multilink propagation channels in amplify-and-forward relay systems,” *Proc. IWonCMM'10*, Beijing, China, Aug. 2010, pp. 1–5.

[31] N. Czink, B. Bandermer, G. Vazquez-Vilar, A. Paulraj, and L. Jalloul, ”July 2008 radio measurement campaign: Measurement documentation,” Tech. Rep., COST 2100 TD(08)620, Oct. 2008.

[32] X. Cheng, C.-X. Wang, D. I. Laurenson, S. Salous, and A. V. Vasilakos, “An adaptive geometry-based stochastic model for non-isotropic MIMO mobile-to-mobile channels,” *IEEE Trans. Wireless Commun.*, vol. 8, no. 9, pp. 4824–4835, Sept. 2009.

[33] X. Cheng, C.-X. Wang, D. I. Laurenson, S. Salous, and A. V. Vasilakos, ”New deterministic and stochastic simulation models for non-isotropic scattering mobile-to-mobile Rayleigh fading channels”, *Wireless Communications and Mobile Computing*, John Wiley & Sons, accepted for publication.

[34] A. Abdi, J. A. Barger, and M. Kaveh, “A parametric model for the distribution of the angle of arrival and the associated correlation function and power spectrum at the mobile station,” *IEEE Trans. Veh. Technol.*, vol. 51, no. 3, pp. 425–434, May 2002.

[35] I. S. Gradshteyn and I. M. Ryzhik, *Table of Integrals, Series, and Products*. 6th ed. Boston: Academic, 2000.

TABLE I. DEFINITION OF PARAMETERS IN FIG. 2.

D_1, D_2, D_3	distances of BS-MS, RS-MS, and BS-RS, respectively
R_{1n_1}, R_{2n_1}; R_{1n_2}, R_{2n_2}; R_{1n_3}, R_{2n_3}	min and max radii of the circular rings around the MS, RS and BS, respectively
θ, θ'	angles between the RS-MS link and BS-MS link, and between the BS-RS link and BS-MS link, respectively
$\delta_1, \delta_2, \delta_3$	antenna element spacings of MS, RS and BS, respectively
$\beta_1, \beta_2, \beta_3$	orientations of the MS, RS and RS antenna arrays in the x-y plane (relative to the x-axis), respectively
$\alpha_{1n_i}, \alpha_{2n_i}$, and α_{3n_i}	azimuth angles of S_{n_i}-MS, S_{n_i}-RS, and S_{n_i}-BS links in the x-y plane (relative to the x-axis), respectively
$\xi^B_{n_1}, \xi^B_{n_2}, \xi^B_{n_3}$	distances d(BS,S_{n_1}), d(BS,S_{n_2}), and d(BS,S_{n_3}), respectively
$\xi^R_{n_1}, \xi^R_{n_2}, \xi^R_{n_3}$	distances d(RS,S_{n_1}), d(RS,S_{n_2}), and d(RS,S_{n_3}), respectively
$\xi^M_{n_1}, \xi^M_{n_2}, \xi^M_{n_3}$	distances d(MS,S_{n_1}), d(MS,S_{n_2}), and d(MS,S_{n_3}), respectively
$\varepsilon_{p_i n_g}(\varepsilon_{n_g p_i})$, $\varepsilon_{p_i p_j}$, and $\varepsilon_{n_g n_k}$	distances $d(p_i, S_{n_g})$, $d(p_i, p_j)$, and $d(S_{n_g}, S_{n_k})$, respectively

TABLE II. MAIN FEATURES OF THE PROPOSED COOPERATIVE MIMO GBSM.

<table>
<tr><th colspan="4">The Proposed Cooperative MIMO GBSM</th></tr>
<tr><td>Links</td><td colspan="3">Three different links: BS-RS, RS-MS, and BS-MS links. (can be easily extended to include more links)</td></tr>
<tr><td rowspan="3">Scenarios</td><td colspan="3">12 cooperative scenarios</td></tr>
<tr><td colspan="2">Physical scenarios</td><td>Application scenarios</td></tr>
<tr><td colspan="2">Outdoor Macro-cell
Outdoor Micro-cell
Outdoor Pico-cell
Indoor scenarios</td><td>BS cooperation
MS cooperation
Relay cooperation</td></tr>
<tr><td rowspan="3">Key Parameters</td><td>I</td><td>$k_{p_3p_2}$
$k_{p_3p_1}$
$k_{p_2p_1}$</td><td>$\eta^{1g}_{p_3p_2/p_3p_1/p_2p_1}$
$\eta^{2g}_{p_3p_2/p_3p_1/p_2p_1}$
$\eta^{31}_{p_3p_2/p_3p_1/p_2p_1}$
$(g = 1, 2, 3)$</td></tr>
<tr><td>The number of local scattering areas.</td><td>Ricean factor of the BS-RS link, BS-MS link, and RS-MS link, respectively.</td><td>Energy-related parameters that specify how much the single-, double-, and triple-bounced rays contribute to the total scattered power of the BS-RS/ BS-MS/ RS-MS link, respectively.</td></tr>
<tr><td colspan="3">By properly adjusting the key parameters, the proposed cooperative MIMO GBSM is suitable for 12 cooperation scenarios.</td></tr>
</table>

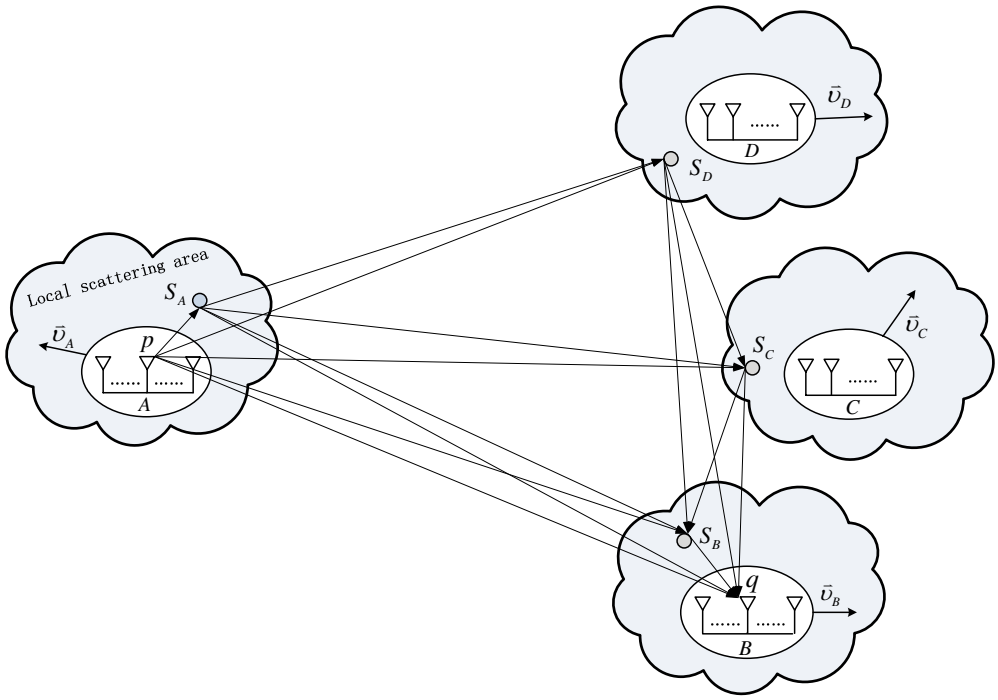

LoS Component	$A_p \to B_q : h_{pq}^{LOS}(t,\tau)$
***i*=1, Single-bounced Components**	$A_p \to S_B \to B_q : h_{pq}^{11}(t,\tau)$ $A_p \to S_C \to B_q : h_{pq}^{12}(t,\tau)$ $A_p \to S_D \to B_q : h_{pq}^{13}(t,\tau)$ $A_p \to S_A \to B_q : h_{pq}^{14}(t,\tau)$
***i*=2, Double-bounced Components**	$A_p \to S_A \to S_B \to B_q : h_{pq}^{21}(t,\tau)$ $A_p \to S_A \to S_C \to B_q : h_{pq}^{22}(t,\tau)$ $A_p \to S_A \to S_D \to B_q : h_{pq}^{23}(t,\tau)$ $A_p \to S_D \to S_B \to B_q : h_{pq}^{24}(t,\tau)$ $A_p \to S_D \to S_C \to B_q : h_{pq}^{25}(t,\tau)$ $A_p \to S_C \to S_B \to B_q : h_{pq}^{26}(t,\tau)$
***i*=3, Triple-bounced Components**	$A_p \to S_A \to S_D \to S_B \to B_q : h_{pq}^{31}(t,\tau)$ $A_p \to S_A \to S_D \to S_C \to B_q : h_{pq}^{32}(t,\tau)$ $A_p \to S_A \to S_C \to S_B \to B_q : h_{pq}^{33}(t,\tau)$ $A_p \to S_D \to S_C \to S_B \to B_q : h_{pq}^{34}(t,\tau)$
***i*=4, Quadruple-bounced Components**	$A_p \to S_A \to S_D \to S_C \to S_B \to B_q : h_{pq}^{41}(t,\tau)$

Fig. 1. Geometry of a unified cooperative MIMO channel model framework.

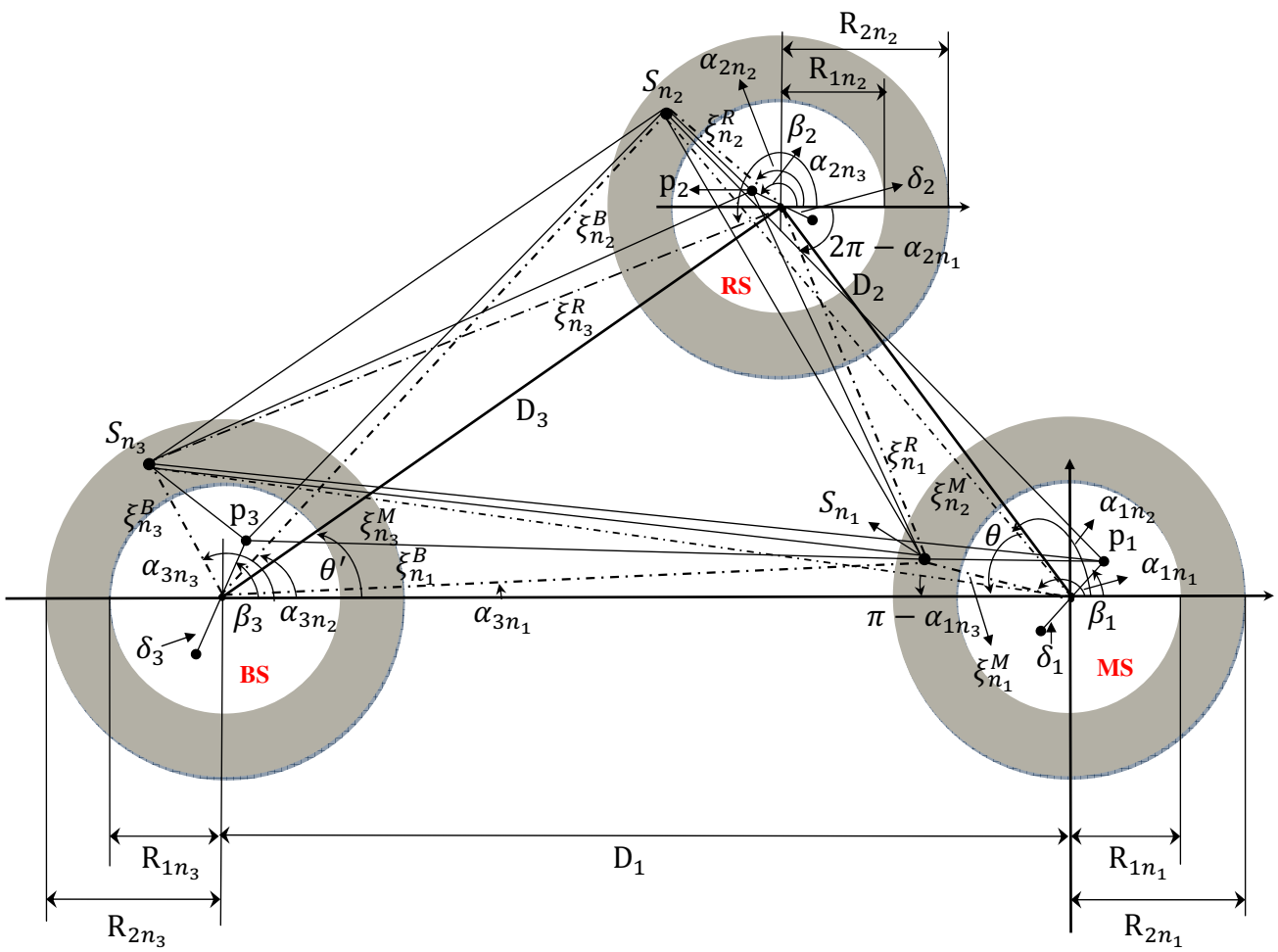

Fig. 2. The proposed cooperative MIMO GBSM.

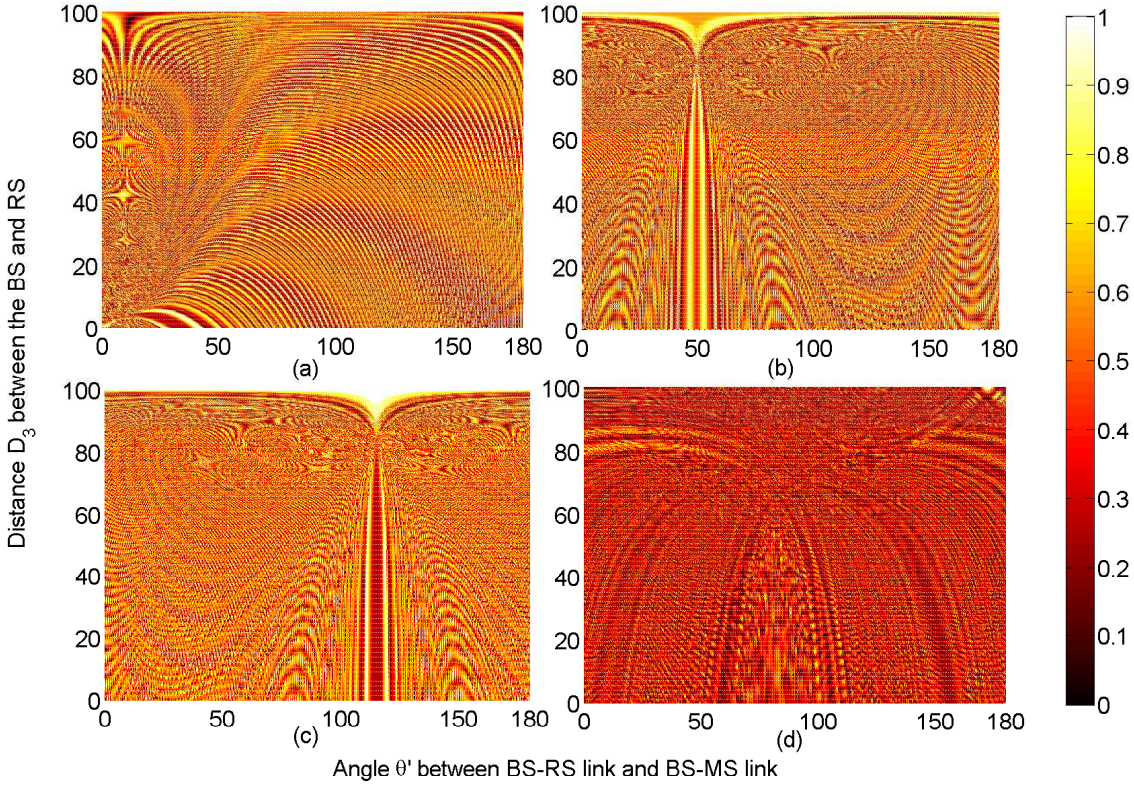

Fig. 3. Absolute values of spatial correlation functions between the BS-RS link and BS-MS link for (a) the first single-bounced component $\rho^{11}_{p_3p_2,p_3'p_1}$; (b) the third single-bounced component $\rho^{13}_{p_3p_2,p_3'p_1}$; (c) the third double-bounced component $\rho^{23}_{p_3p_2,p_3'p_1}$; and (d) the triple-bounced component $\rho^{31}_{p_3p_2,p_3'p_1}$.

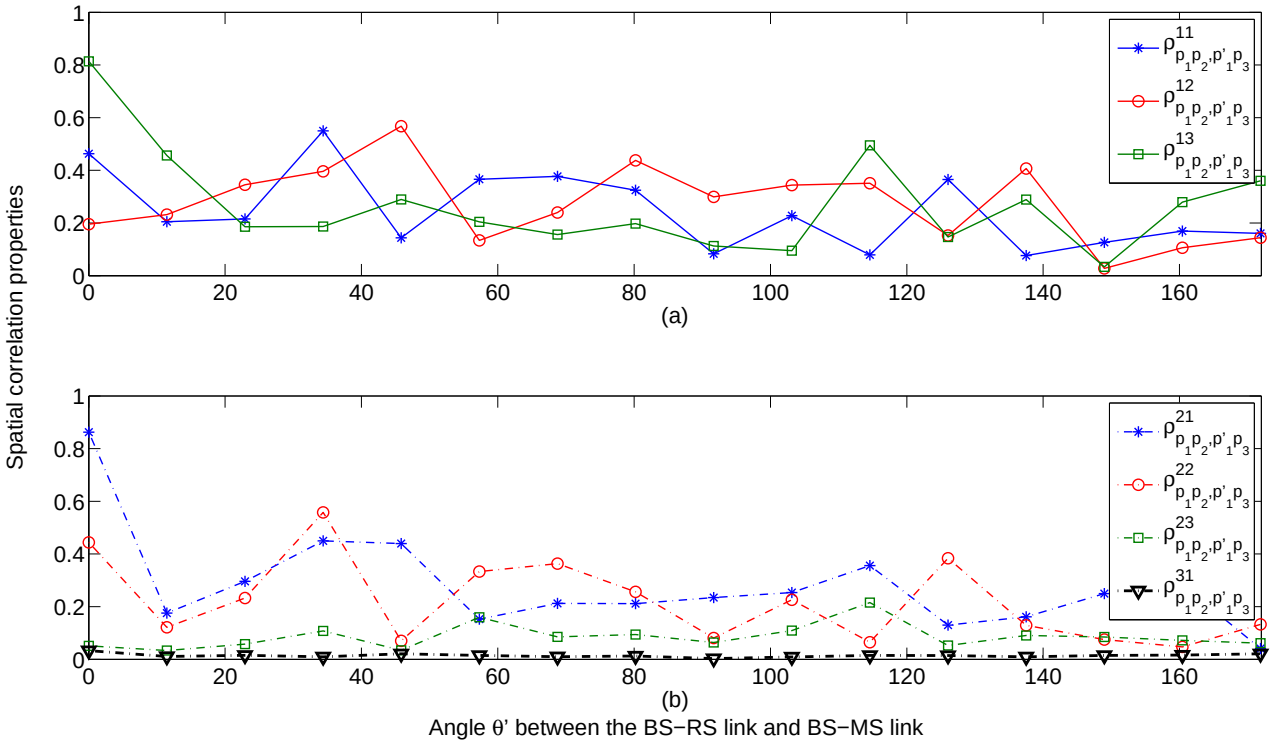

Fig. 4. Absolute values of spatial correlation functions between the BS-RS link and BS-MS link for (a) the single-bounced components and (b) the double- and triple-bounce components.

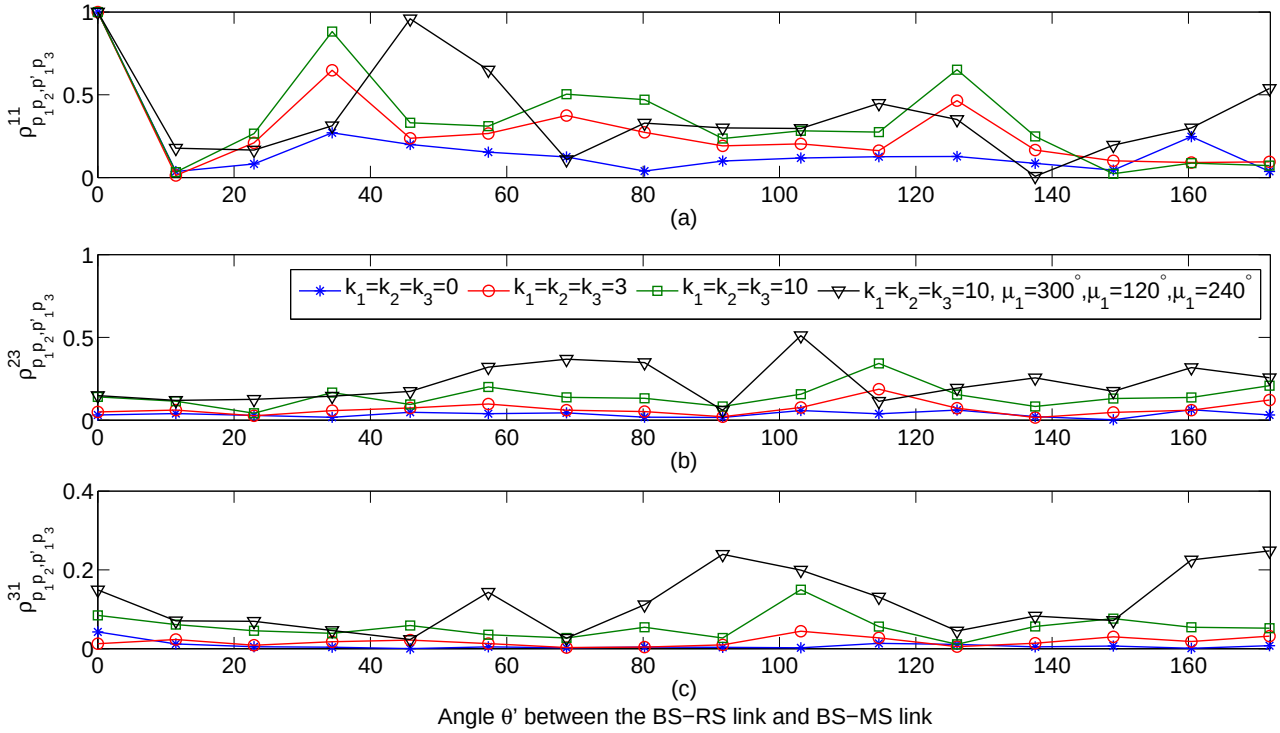

Fig. 5. Absolute values of spatial correlation functions between the BS-RS link and BS-MS link for (a) the first single-bounced component $\rho^{11}_{p_3p_2,p'_3p_1}$; (b) the third double-bounced component $\rho^{23}_{p_3p_2,p'_3p_1}$; and (c) the triple-bounced component $\rho^{31}_{p_3p_2,p'_3p_1}$ with different values of parameters k_g and μ_g $(g = 1, 2, 3)$.

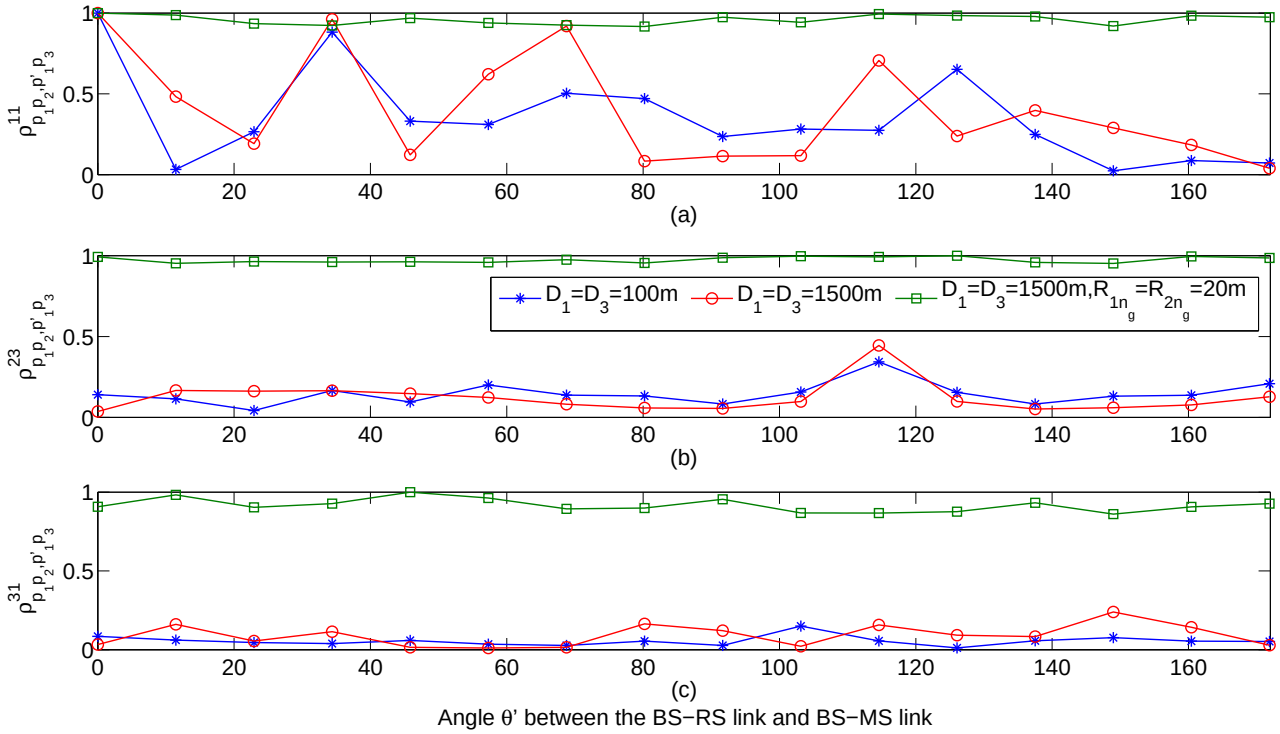

Fig. 6. Absolute values of spatial correlation functions between the BS-RS link and BS-MS link for (a) the first single-bounced component $\rho^{11}_{p_3p_2,p_3'p_1}$; (b) the third double-bounced component $\rho^{23}_{p_3p_2,p_3'p_1}$; and (c) the triple-bounced component $\rho^{31}_{p_3p_2,p_3'p_1}$ with different values of parameters D_3, R_{1n_g}, and R_{2n_g} $(g = 1, 2, 3)$.

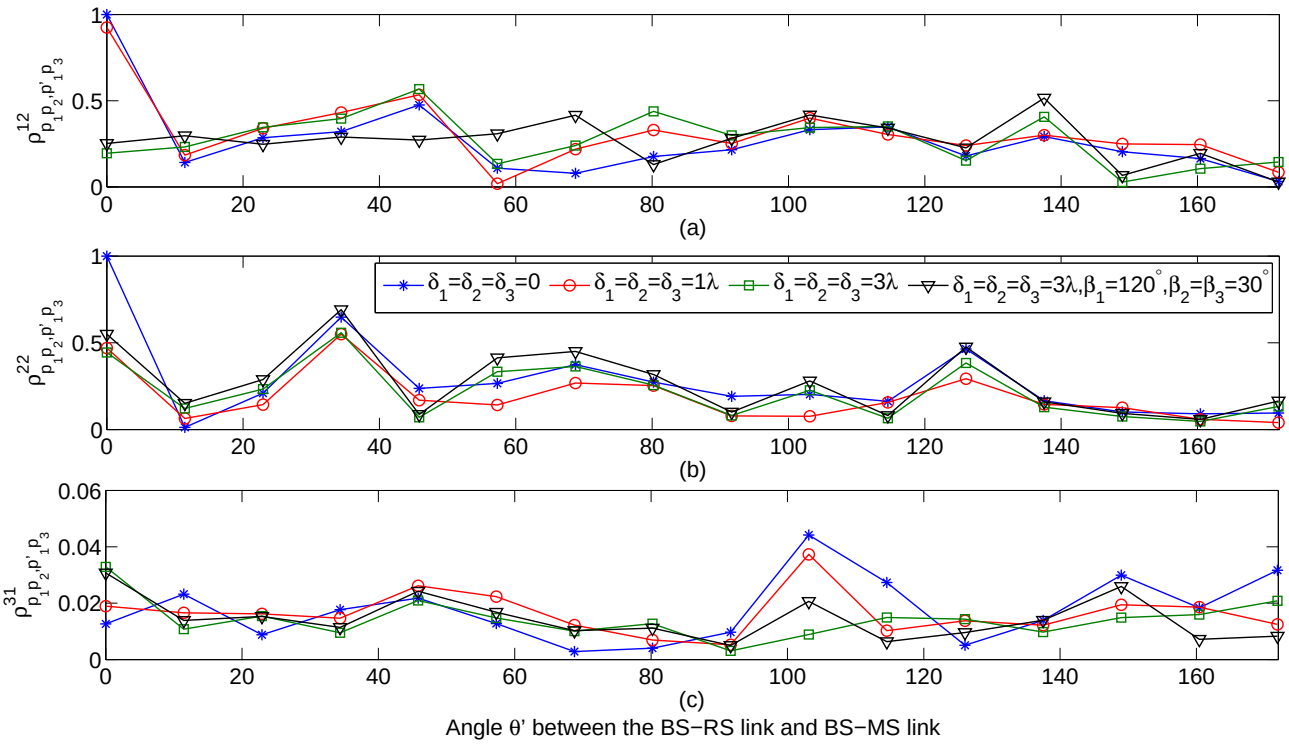

Fig. 7. Absolute values of spatial correlation functions between the BS-RS link and BS-MS link for (a) the second single-bounced component $\rho^{12}_{p_3p_2,p'_3p_1}$; (b) the second double-bounced component $\rho^{22}_{p_3p_2,p'_3p_1}$; and (c) the triple-bounced component $\rho^{31}_{p_3p_2,p'_3p_1}$ with different values of parameters δ_g and β_g ($g = 1, 2, 3$).

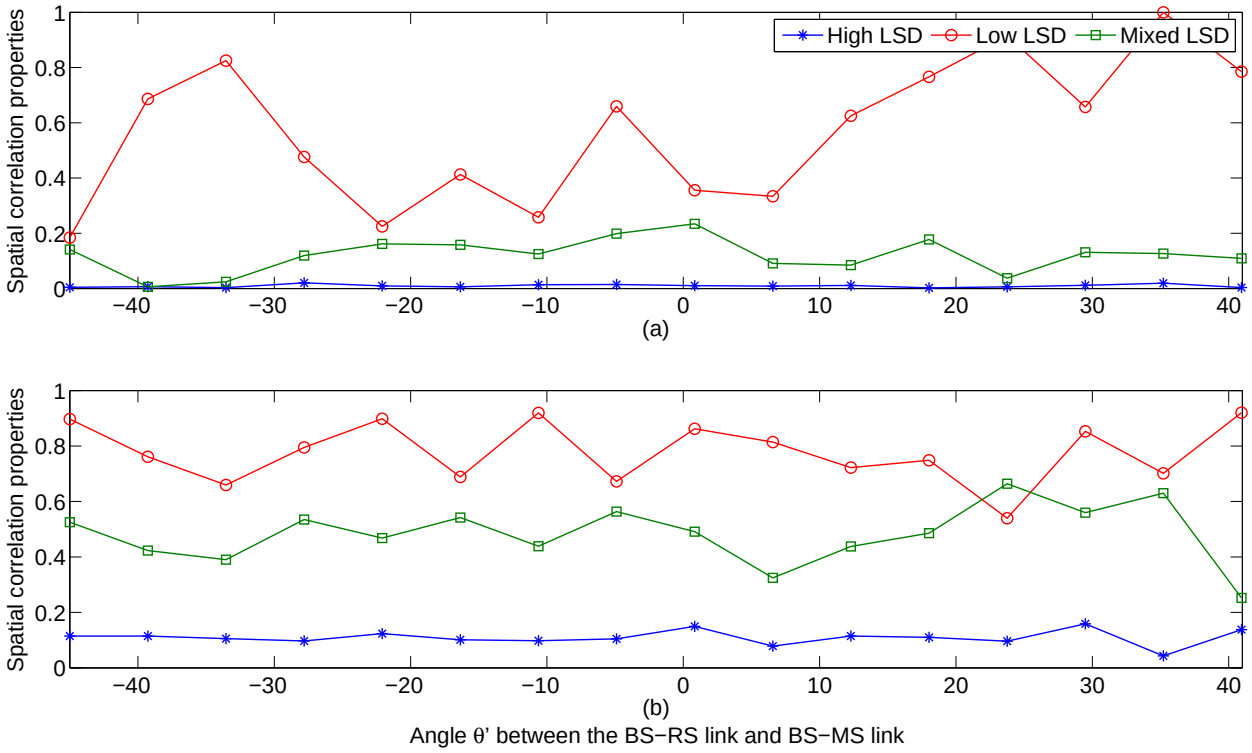

Fig. 8. Absolute values of spatial correlation functions between the BS-RS link and BS-MS link for (a) the outdoor macro-cell MS cooperation scenario and (b) the indoor MS cooperation scenario with different LSDs.